CFD Investigation of Multi-element Airfoils in Wingsails

Shreyas Gowrishankar Chandhavar

Department of Energy Sciences

Lund University, Faculty of Engineering

University Supervisor: Robert-Zoltan Szasz

University Examiner: Xue-Song Bai

MVKM05 - Master Thesis in Sustainable Energy Engineering 30 ECTS

Seminar date: 01-06-2026

ISRN LUTMDN/TMHP-26/5688-SE ISSN 0282-1990

Abstract

Wind-assisted ship propulsion is being studied as a means to reduce a ship's fuel consumption and emissions by using wind energy to provide auxiliary thrust. Rigid wingsail is a rising application because it generates aerodynamic forces in a more controlled manner than flexible sails. However, the performance of the wingsail depends on the airfoil geometry, flap settings, apparent wind direction, and the balance between useful thrust and side force.

This thesis investigates the aerodynamic performance of a NACA 0018-based rigid wingsail with hinged-flap and gap configurations using Computational Fluid Dynamics. Two-dimensional steady Reynolds-Averaged Navier Stokes simulations were performed in OpenFOAM using the SST k–ω turbulence model. The numerical setup was first validated for the plain NACA 0018 airfoil and was then applied to investigate the influence of flap deflection, hinge position, and gap size on the aerodynamic coefficients and flow behaviour. In addition, the wingsail orientation was analyzed to identify operating conditions that can produce larger thrust.

The validation results showed that the OpenFOAM setup reproduced the main lift and drag trends of the plain airfoil over the investigated angle-of-attack range. The hinged-flap results showed that increasing flap deflection increased lift by increasing the effective camber of the airfoil, but this was also accompanied by an increase in drag in several cases. The hinge position affected the aerodynamic behaviour by changing the effective flap length, although its influence was less consistent than that of flap deflection. The gap sensitivity analysis showed that the investigated gap configurations increased drag and did not improve overall aerodynamic efficiency relative to the plain-airfoil baseline.

The wingsail-orientation analysis showed that the highest lift condition is not necessarily the most useful condition for ship propulsion. This is because both lift and drag can contribute to thrust, depending on the apparent wind direction and sail orientation. Therefore, the aerodynamic forces were resolved into thrust and side-force components to identify operating conditions with high useful thrust and manageable side force.

Due to the limited available project time and computational resources, only two-dimensional simulations were carried out. Therefore, the results should be interpreted as sectional aerodynamic trends rather than full ship performance predictions.

Keywords: Wind-assisted ship propulsion, rigid wingsail, hinged flap, NACA 0018, OpenFOAM, CFD, RANS, SST k–ω

Acknowledgement

The author would like to express sincere gratitude to the supervisor, Robert-Zoltan Szasz, for his guidance, feedback, and support throughout this thesis work. His suggestions helped improve the structure, technical quality, and clarity of the project.

The author would also like to thank Lund University and the Department of Energy Sciences for providing the opportunity to carry out this master's thesis. The knowledge and experience gained during the programme have been valuable for the author's academic and professional development.

The author is thankful to the teachers, classmates, and friends who provided support during different stages of the thesis. Their discussions, encouragement, and help made the work easier to complete.

The author would also like to thank their family for their constant support, patience, and motivation throughout the study period. Their encouragement has been very important during this journey.

Finally, the author would like to acknowledge the use of open-source tools, including OpenFOAM and ParaView, for CFD simulations and post-processing in this project.

AI Use

During the thesis work, various AI-based and digital tools were used to support writing, editing, reference management, and document formatting. Grammarly was used to correct grammar, spelling, sentence structure, and readability. However, the author checked the suggested changes to ensure that the original meaning of each sentence was not altered. A thesaurus and a dictionary were used to check word meanings, improve word choice, and avoid repetition.

NotebookLM was used as a reading and learning support tool after uploading research papers and thesis-related documents. It was mainly used to ask questions about papers the author had already read. For example, when the distinction between a high-lift device and a multi-element airfoil was unclear, NotebookLM was used to explain the concept more simply. Follow-up questions were then asked to improve the author's understanding of the topic.

ChatGPT was mainly used as a technical writing and formatting support tool. It was used to convert manually written content into LaTeX code for Overleaf, including equations, symbols, figure layouts, tables, and section formatting. The author first wrote or planned the content manually, and then used ChatGPT to convert it into the correct LaTeX format.

ChatGPT was also used to generate Python scripts to plot graphs and arrange contour

figures, as preparing these manually in Excel or other software was time-consuming. The aerodynamic data, contour plots, and simulation results themselves were not generated by AI. They were obtained from OpenFOAM and post-processing tools. AI was only used to help organize, plot, or format the results.

No images in the thesis were generated using AI. Some advice was obtained from ChatGPT on how to cite open-source images correctly and format figures in the document. ChatGPT was also used to get suggestions on document formatting, including the table of contents, keywords, figure placement, and the overall thesis structure.

All AI-assisted outputs were reviewed, edited, and approved by the author. The CFD simulations, interpretation of results, final analysis, and academic decisions were carried out solely by the author.

CONTENTS

List of Figures

List of Tables

Nomenclature

AI Artificial intelligence

AoA Angle of attack

AWA Apparent wind angle

BL Boundary layer

CFD Computational fluid dynamics

DNS Direct numerical simulation

FV Finite volume

GAMG Geometric-algebraic multigrid

GHG Greenhouse gas

IMO International Maritime Organization

LE Leading edge

LES Large-eddy simulation

NACA National Advisory Committee for Aeronautics

RANS Reynolds-averaged Navier–Stokes

SIMPLE Semi-Implicit Method for Pressure-Linked Equations

SST Shear Stress Transport

STL Stereolithography

TE Trailing edge

WASP Wind-assisted ship propulsion

A_{ref} Reference area, [m^2]

b Reference span, [m]

c Chord length, [m]

C_D Drag coefficient, [-]

C_L Lift coefficient, [-]

$C_{L,\max}$ Maximum lift coefficient, [-]

C_M Moment coefficient, [-]

C_S Side-force coefficient, [-]

C_T Thrust coefficient, [-]

D Drag force, [N]

F_x Force component in the x-direction, [N]

F_y Force component in the y-direction, [N]

g Gap size between the main element and flap element, [m]

g/c Gap-to-chord ratio, [-]

k Turbulent kinetic energy, [$\mathrm{m}^2/\mathrm{s}^2$]

L Lift force, [N]

M Aerodynamic moment, [N m]

N_{cells} Number of computational cells, [-]

q_∞ Free-stream dynamic pressure, [N/m^2]

Re Reynolds number, [-]

T Thrust force, [N]

U_∞ Free-stream velocity, [m/s]

x/c Non-dimensional chordwise position, [-]

y^+ Non-dimensional wall distance, [-]

α Angle of attack, [°]

β Apparent wind angle, [°]

δ Flap deflection angle, [°]

ΔC_D Change in drag coefficient, [-]

ΔC_L Change in lift coefficient, [-]

θ Sail orientation angle, [°]

ρ Air density, [kg/m^3]

ω Specific dissipation rate, [s^{-1}]

1 Introduction

1.1 Background

1.1.1 Environmental and Economic Drivers for Sustainable Shipping

International shipping is an important component of global logistics and facilitates approximately 90% of world trade by volume, Von Klemperer et al. (2023). However, the shipping sector still relies heavily on traditional fossil fuels and is responsible for approximately 3% of total global greenhouse gas (GHG) emissions, equivalent to approximately 940 million tonnes of CO_2 annually, Xu et al. (2025). In response to this issue, the International Maritime Organization (IMO) has introduced targets to reduce carbon intensity by at least 40% by 2030 and to reach net-zero GHG emissions by 2050, Xu et al. (2025). In addition to environmental regulations, fuel consumption is an important economic burden, as fuel typically accounts for 40%–60% of total ship operating costs, Von Klemperer et al. (2023).

1.1.2 Wind-Assisted Ship Propulsion as an Alternative

The transition to sustainable energy sources has renewed interest in Wind-Assisted Ship Propulsion (WASP), which supplements conventional engine propulsion with wind energy. WASP systems, such as rotor sails, suction sails, and wingsails, typically do not replace the main engine but instead reduce required propulsive power by providing auxiliary thrust, Malmek et al. (2024). These technologies are discussed in more detail in Section 2.1. Industry data indicate that these systems can achieve fuel savings of approximately 5%–20%, with peak reductions exceeding 30% under favourable weather conditions, Von Klemperer et al. (2023). As of 2025, adoption of these technologies has increased, with approximately 52 ships in operation and 97 additional ships on order, Hoffmeister et al. (2025).

1.1.3 Aerodynamic Efficiency of Wingsails and Hinged Flaps

Among emerging wind-assisted technologies, wingsails are notable for functioning as rigid aerodynamic lifting surfaces. Their operation relies on airfoil theory, generating aerodynamic forces through pressure differences across the profile, Ma et al. (2025). Unlike traditional soft fabric sails, rigid wingsails maintain a stable airfoil shape during operation, enabling more predictable aerodynamic performance and higher lift-to-drag ratios,

also known as glide ratios, Xu et al. (2025).

The aerodynamic performance of a wingsail is significantly affected by its geometry, especially the camber of the airfoil section. Cambered airfoils can generate greater lift than symmetric profiles at the same angle of attack; however, a fixed camber may not be optimal for all apparent wind directions. Hinged trailing-edge (TE) flaps are employed to change the effective camber of the wingsail. Adjusting flap deflection and hinge position allows control over lift, drag, and thrust-producing force for various operating conditions, Von Klemperer et al. (2023). Research on articulated wingsails demonstrates that improving hinge position can increase the maximum lift coefficient, $C_{L,\max}$, compared to a fixed profile of the same cross-section, Von Klemperer et al. (2023).

1.2 Problem Statement

Rigid wingsails represent a promising technology for WASP due to their ability to generate aerodynamic forces that supplement conventional ship propulsion, Jiang et al. (2024); Von Klemperer et al. (2023). Their effectiveness, however, is highly dependent on sail geometry and operating conditions, including the apparent wind angle (AWA), Jiang et al. (2024); Ma et al. (2025). While rigid wingsails maintain a stable aerodynamic shape, they lack the adaptability of soft fabric sails to changing wind conditions, Von Klemperer et al. (2023). To address this limitation, hinged flaps are introduced to modify the effective camber and control aerodynamic force generation, Ahmed et al. (2013); Hoffmeister et al. (2025); Von Klemperer et al. (2023).

Although hinged flaps can enhance lift, their impact on overall propulsion performance is not uniformly positive. Excessive flap deflections or suboptimal hinge positions may increase aerodynamic drag and diminish the useful thrust generated by the sail, Jiang et al. (2024); Kamliya Jawahar et al. (2018); Von Klemperer et al. (2023). Consequently, the configuration yielding the highest lift does not necessarily correspond to the most effective arrangement for ship propulsion, Jiang et al. (2024); Von Klemperer et al. (2023).

Because the lift direction is typically not aligned with the ship heading, the effects of hinge position and flap deflection must be assessed using not only lift and drag coefficients but also the thrust-producing force component and associated flow behaviour, Jiang et al. (2024); Ma et al. (2025). A comprehensive understanding of these factors is essential for identifying wingsail configurations that enhance aerodynamic performance while providing

useful thrust by keeping the side forces, flow separation, and the aerodynamic loading under reasonable limits. Ma et al. (2025); Zhang et al. (2025).

1.3 Aim of the Study

This thesis aims to investigate the aerodynamic performance of multi-element wingsail airfoils equipped with hinged trailing-edge flaps using Computational Fluid Dynamics (CFD). The research focuses on the effects of angle of attack (AoA), flap deflection angle, hinge position, and gap size on lift, drag, thrust-related force, and overall aerodynamic behavior. Additionally, the thesis seeks to develop and validate an OpenFOAM-based CFD workflow for comparing various wingsail configurations.

1.4 Research Objectives

The objectives of this thesis are:

1. Develop a two-dimensional CFD workflow for NACA 0018 airfoils using OpenFOAM. This includes geometry preparation, mesh generation, boundary condition definition, solver selection, and convergence assessment.

2. Validate the baseline CFD setup by comparing numerical results with published aerodynamic data for the plain NACA 0018 airfoil. This validation determines whether the CFD method accurately reproduces the primary lift, drag, pressure, and stall characteristics before application to modified wingsail configurations.

3. Examine the influence of hinged flap deflection angle and hinge position on the aerodynamic characteristics of the wingsail airfoil, comparing configurations based on lift, drag, and flow behavior.

4. Investigate the influence of the gap between the main element and flap element of a two-element airfoil, as gap size is expected to affect aerodynamic forces and flow interaction compared with the plain NACA 0018 baseline airfoil.

5. Evaluate the thrust-related force component for selected apparent wind directions, recognizing that the lift force is not necessarily aligned with the ship-forward direction.

1.5 Scope and Limitations

Due to the limited available computing resources and the large number of configurations considered in this thesis, the study was restricted to two-dimensional simulations. A two-dimensional approach enabled comparison of several angles of attack, flap deflections, hinge positions, and gap configurations within the available project time. This was considered suitable because the main objective of the thesis was to compare aerodynamic trends between different wingsail airfoil configurations, rather than to predict the complete full-scale performance of a ship-mounted wingsail.

The simulations were executed using Reynolds-Averaged Navier–Stokes (RANS) modelling with the SST k–ω turbulence model in OpenFOAM. This approach provided a practical balance between computational cost and fluid-dynamic accuracy for the present comparative study. The two-dimensional RANS setup was used to evaluate the lift coefficient C_L, the drag coefficient C_D, the moment coefficient C_M, the maximum lift coefficient $C_{L,\max}$, the lift-to-drag ratio C_L/C_D, the thrust coefficient C_T, the side-force coefficient C_S, and selected pressure and velocity contours.

The study includes a baseline validation case and a limited parametric analysis of articulated flap configurations. The main parameters considered are angle of attack, flap deflection angle, hinge position, and selected gap sizes. The gap study compares two selected two-element gap configurations, $g/c = 0.018$ and $g/c = 0.028$, with the plain NACA 0018 baseline.

However, the two-dimensional RANS approach also introduces limitations. Three-dimensional effects, such as tip vortices, spanwise flow, finite-span effects, and interaction with the ship deck and superstructure, are not captured. In addition, structural deformation, fluid–structure interaction, ship-motion effects, and direct coupling with a complete vessel model are outside the scope of this work.

Therefore, the results should be interpreted as two-dimensional aerodynamic trends rather than complete full-scale ship performance predictions. The results are useful for comparing the relative influence of flap deflection, hinge position, gap size, and apparent wind orientation, but further three-dimensional and ship-level studies are required before applying the findings directly to practical wingsail design.

2 Literature Review

2.1 Wind Assisted Ship Propulsion

The wind-assisted ship propulsion (WASP) refers to technologies that use the wind energy to support the main propulsion system of a ship. These systems do not replace the main conventional engine but can also reduce the required engine power by producing additional aerodynamic thrust force. In this regard, WASP can contribute to the lower fuel consumption and reduce emissions depending upon the ship type, route, apparent wind conditions and control strategy, Gaul and Rutkowski (2025); Von Klemperer et al. (2023).

There are several WASP technologies that have been proposed and tested for maritime applications. These included the rotor sails, soft sails, rigid wingsails, suction sails and multi-element or hinged wingsails. Although all these systems use the wind as an additional source of energy, the aerodynamic principles and practical implementations are very different. Figure 1 shows the main types of WASP technologies, which are discussed in this review.

2.1.1 Rotor Sails

Rotor sails, also known as Flettner rotors, are vertical rotating cylinders mounted on the ship's deck. Their operation is based on the Magnus effect, where a rotating body placed in an incoming flow generates a force that is perpendicular to the flow direction. When the rotor spins in the apparent wind, the velocity distribution around the cylinder becomes asymmetric. This creates a pressure difference between the two sides of the rotor and produces the aerodynamic lift force, Seifert (2012).

For the propulsion of the ship, the lift produced by the rotor is useful only when part of it acts in the forward direction of the ship. Therefore, the effectiveness of a rotor sail depends strongly on the AWA, the rotational direction, and the spin of the rotor. The spin ratio describes the relation between the surface speed of the rotating cylinder and the incoming wind speed. The higher spin ratios can increase the lift force, but they also require more power and may increase the practical limitations related to control and efficiency, De Marco et al. (2016); Khan et al. (2021).

Compared with traditional soft fabric sails, rotor sails can be controlled by varying

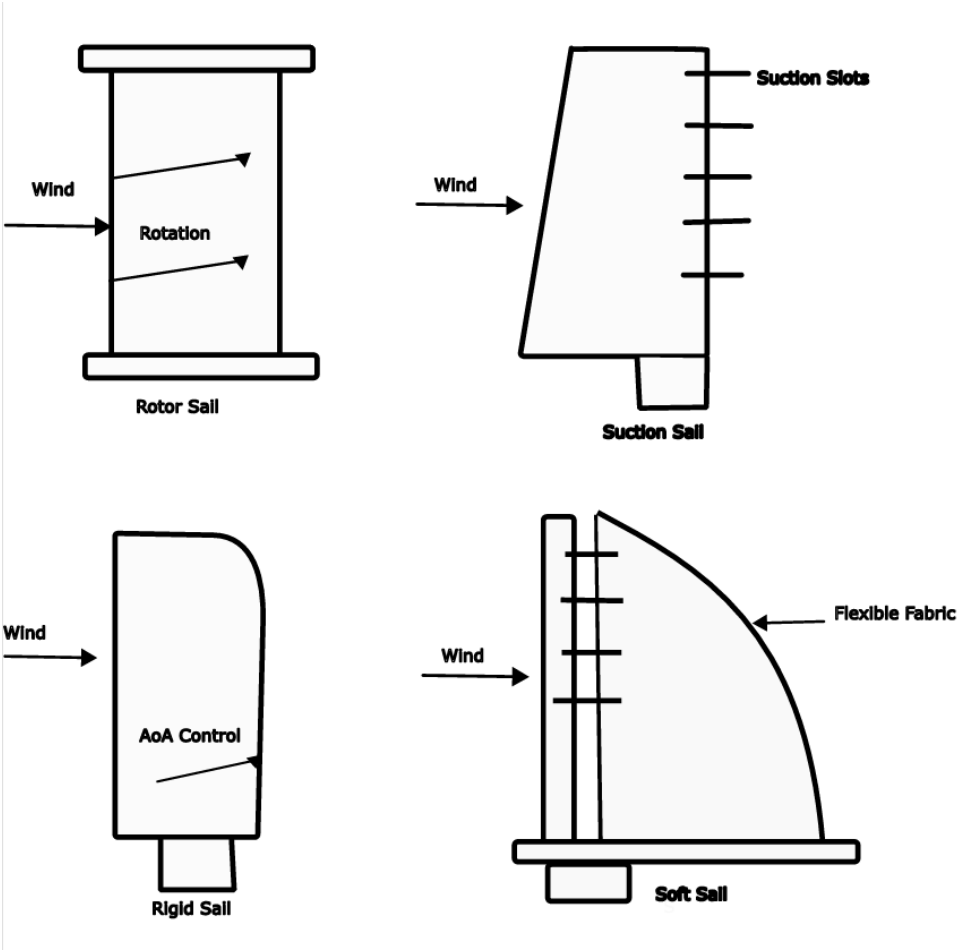

Figure 1: Various types of WASP Technologies. Source : Reproduced after Hoffmeister et al. (2025)

their rotational speed. However, they require electrical power to rotate and generate aerodynamic drag during operation Khan et al. (2021). When it is inactive, it may still add resistance unless it is folded or tilted, depending on its design. Their height, weight, and deck space requirements affect the ship's stability, visibility, and cargo operations, Zhang et al. (2025).

2.1.2 Soft Sails and Rigid Wingsail

Soft sails are flexible fabric-based sails whose shapes can change under aerodynamic loading. Their exposed area and aerodynamic loading can be reduced by reefing or trimming the sail. However, this flexibility implies that the sail profile changes under aerodynamic loading, which often leads to loss of propulsion efficiency. Due to this reason, the soft sail is sensitive to wind conditions, fabric deformations, and control settings, Chen et al. (2018).

Rigid wing sails, also referred to as hard sails, are vertical airfoil-shaped structures mounted on a ship's deck. Unlike the soft sails, rigid sails maintain a fixed and stable profile under operations, Gaul and Rutkowski (2025). It is important because the aerodynamic forces produced by the sail depend strongly on the shape of the profile and its relative angle to the incoming apparent wind. A rigid wingsail produces more predictable lift and drag behaviour than a flexible sail, Ma et al. (2025); Xu et al. (2025).

A single-element wingsail is the simplest type of rigid wingsail. It consists of a single continuous aerodynamic element without any separate flap, slat, slot, or gap. This single-element wingsail is useful as a reference or validation case before studying more complex wingsail designs like the hinged articulated flap or any multi-element wingsail configurations, Von Klemperer et al. (2023); Fang et al. (2024).

In addition to the single-element rigid wingsail, more advanced rigid wingsail concepts include hinged flaps or multiple aerodynamic elements to modify the effective camber and improve aerodynamic performance. These concepts related to high-lift devices, including trailing-edge flaps, multi-element configurations, and flow controls, are discussed in 2.4.

2.1.3 Suction Sails

Suction sails, also known as suction wings or Ventifoils, are vertical airfoil-shaped structures that are mounted on the ship's deck in order to generate auxiliary propulsive force

from the wind, Seifert (2012). Unlike the rotor sails, suction sails do not rely on the Magnus effect because their outer surfaces remain stationary, Gaul and Rutkowski (2025). However, their operating principle is based on active boundary layer control, which means they use internal fans or suction systems to control airflow and enhance propulsive force. Their useful thrust depends on the apparent wind direction; they generate little useful thrust when the apparent wind comes mainly from either the forward or rearward directions of the ships, Kolodziejski and Sosnowski (2025).

2.2 Aerodynamic Fundamentals and Boundary Layers

This section will discuss the airfoil nomenclature, relevant forces and the respective aerodynamic coefficients, boundary layer (BL) theory, adverse pressure gradients, flow separation, stall, and its characteristics which will provide a basic fundamental knowledge. An airfoil (see Figure 2) is defined as a cross-sectional shape of a wing, which is taken parallel to the flow direction. The airfoil geometry is described by several standard parameters. The leading edge (LE) is the frontmost point of the airfoil, whereas the trailing edge (TE) is the rearward point where the upper and lower surfaces of the airfoil meet. The chord line is a straight line connecting the LE and TE, and the chord length c is the distance between the LE and TE points. The mean camber line is a curve formed by the locus of points that is located in the middle of the upper and lower surfaces of the airfoil. The camber is the maximum distance between the mean camber line and the chord line, which is measured perpendicular to the chord line. The angle of attack (AoA, α) is the angle between the chord line and the relative wind direction, Anderson (2017).

The aerodynamic forces acting on the airfoil (Figure 3) are mainly produced by pressure and viscous shear stress. The pressure acts normal to the airfoil surface, while shear stress acts tangentially along the point of the airfoil surface. When these forces are integrated, they produce the resultant aerodynamic forces: lift and drag. Lift (L) is the force that acts perpendicular to the wind direction, and the drag (D) force acts parallel to the wind direction. In addition to these fundamental forces, the pressure distribution also produces a pitching moment (M) that rotates the airfoil and tends to change the AoA. These forces have respective dimensionless coefficients that are used to compare forces and moments across different configurations. For a two-dimensional airfoil, the lift and drag are expressed per unit span. Anderson (2017)

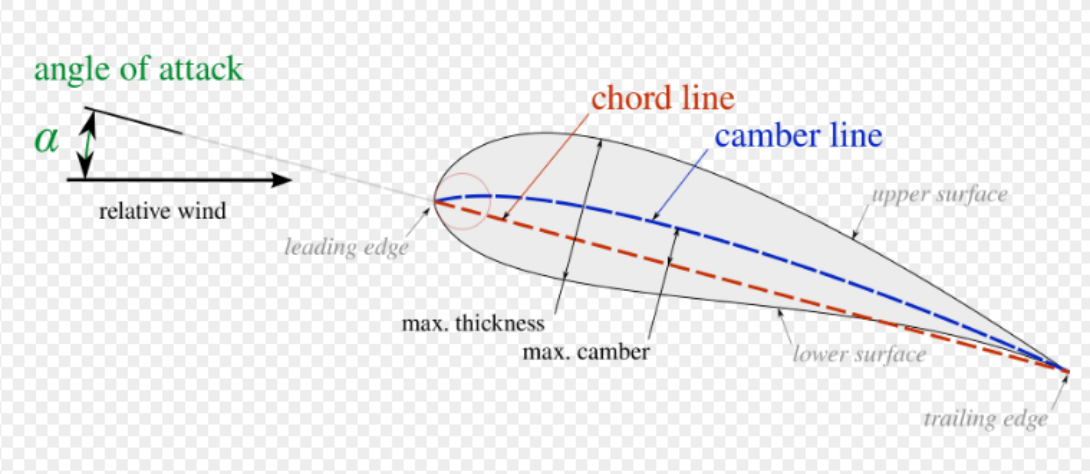

Figure 2: Airfoil nomenclature. Source: Wikimedia Commons, *Wing profile nomenclature*, CC0 1.0 Public Domain.

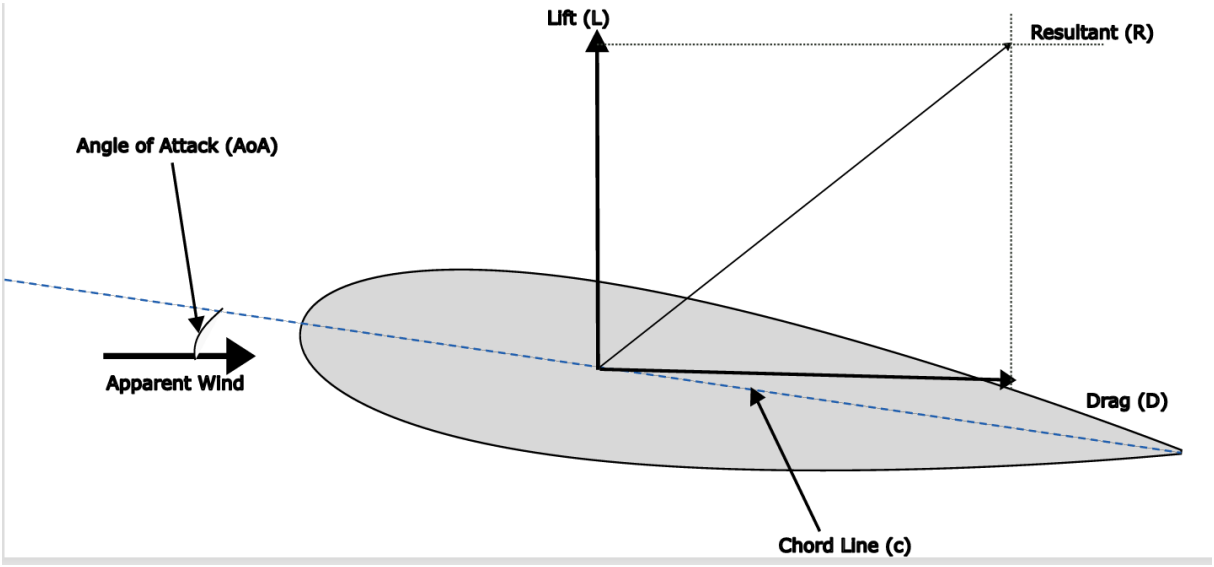

Figure 3: Forces acting on the airfoil

The aerodynamic coefficients were calculated from the aerodynamic forces obtained using OpenFOAM. The lift, drag, and momentum coefficients are defined as:

$$C_L = \frac{L}{q_\infty A_{\text{ref}}} \tag{1}$$

$$C_D = \frac{D}{q_\infty A_{\text{ref}}} \tag{2}$$

$$C_M = \frac{M}{q_\infty A_{\text{ref}} c} \tag{3}$$

where C_L is the lift coefficient, C_D the drag coefficient, and C_M the moment coefficient. The terms L and D are the lift and drag forces, respectively, while M is the aerodynamic moment. The reference area is denoted by A_{ref}, the chord length by c, and the free-stream dynamic pressure by q_∞.

The dynamic pressure is defined as:

$$q_\infty = \frac{1}{2}\rho U_\infty^2 \tag{4}$$

where ρ is the air density and U_∞ is the free-stream velocity.

Boundary layer theory is vital to understanding the airfoil performance because the viscous effects dominate at the airfoil surface. The boundary layer is a thin region of flow near the wall where viscosity has a tremendous effect. At the airfoil surface, the no-slip condition requires the fluid to be zero relative to the wall. With increasing distance away from the wall, the velocity increases until it reaches the outer flow velocity, where the viscous effects are much weaker, and the flow is treated as inviscid flow as the flow reaches outside the BL, (Schlichting and Gersten (2017); Vos and Farokhi (2015)).

As the fluid flows over the airfoil surface, it may experience adverse pressure gradients, which occur when the static pressure increases in the flow direction near the TE of the airfoil. Under such conditions, the near-wall flow loses its momentum, and if the pressure rise is strong enough, the flow slows and reverses direction. This point is the beginning point of the flow separation (see Figure 4). After separation, the flow separates from the airfoil surface and forms a recirculation zone with unsteady vortex structures, Schlichting and Gersten (2017).

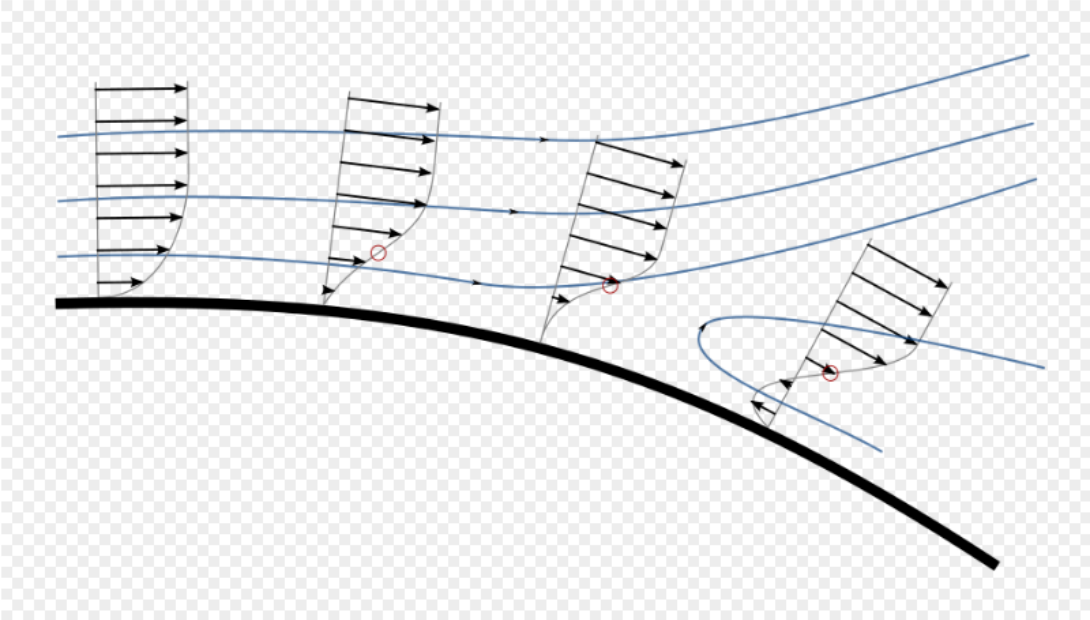

Figure 4: Schematic illustration of boundary-layer separation. Source: Olivier Cleynen, Wikimedia Commons, *Boundary layer separation*, licensed under CC BY 3.0.

The stall of an airfoil is a major concept in aerodynamics, as it indicates the airfoil's limiting capacity. Stall occurs when flow separation becomes too large, causing a sudden loss of lift ,Anderson (2017). It happens when the airfoil exceeds a certain AoA called as the stall angle. As the AoA increases, the adverse pressure gradient strengthens, and the separation regions continue to grow. There are several factors influencing stall, like airfoil geometry, thickness, and LE shape. For thicker airfoils, the TE stall is very common, in which separation starts near the TE and gradually moves forward as AoA increases, Morris and Rusak (2013); Vos and Farokhi (2015).

2.3 Rigid Wingsail Aerodynamics

A rigid wingsail, as discussed in the previous subsection, is a vertical airfoil-shaped structure that uses the apparent wind to generate the aerodynamic forces. A rigid wingsail is not changing due to interaction with the flow, which makes it easier to study using CFD analysis (compared to soft sails). Wingsails are suitable for aerodynamic analysis because their fixed airfoil shape allows the aerodynamic forces to be defined more clearly than in flexible, soft sails. The lift and drag forces are first defined relative to the apparent wind direction. For ship propulsion, these forces can then be resolved into thrust and side-force components relative to the ship heading. This makes it possible to evaluate not only the total aerodynamic force, but also how much of that force contributes to forward

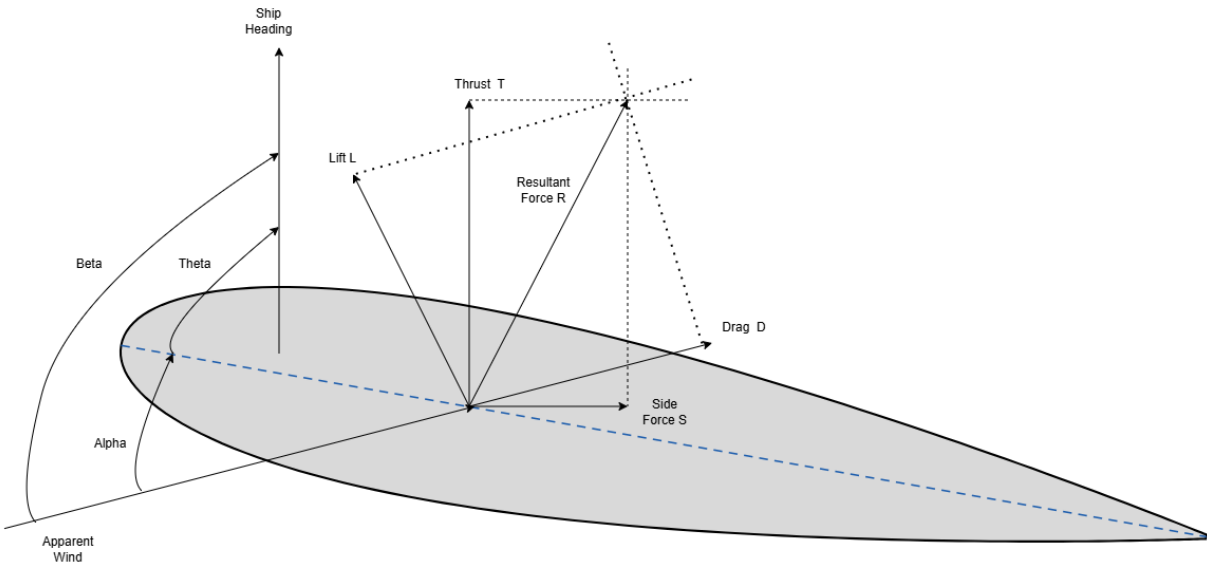

Figure 5: Force decomposition for a rigid wingsail

propulsion and how much acts sideways on the vessel, (Jiang et al., 2024; Fang et al., 2024). The aerodynamic forces are based on the apparent wind, which is a result of the wind created by the forward motion of the ship and the environmental wind,Ma et al. (2025). Therefore, the apparent wind speed and direction depend on the true wind, ship speed, and sailing direction.

In the force diagram (Figure 5), the apparent wind direction is used as the reference direction for the lift and drag. The AoA α is the angle between the airfoil chord line and incoming apparent wind direction. The AWA β is the angle between the apparent wind direction and the ship heading. The sail orientation angle θ represents the rotation of the wingsail chord line relative to the ship heading. These are important because studying the aerodynamic forces determines the useful thrust and side force.

When the apparent wind flows around the wingsail, a resultant aerodynamic force is generated, Jiang et al. (2024). For ship propulsion, this resultant force has to be decomposed relative to the ship's heading. The component acting in the ship's forward direction is the thrust force F_T; it contributes to propulsion and reduces the main engine's power requirement. The side force F_S is acting perpendicular to the ship head and must be balanced by the hull, rudder, etc. Makram et al. (2023). It is also important to note that the wingsails are also generating moments, which are important for the vessel's stability; however, this is not in the scope of the thesis.

The wingsail orientation study was included to assess how the same aerodynamic

force can have different propulsive effects depending on its direction relative to the ship's heading. Although lift and drag describe the aerodynamic performance of the airfoil relative to the apparent wind, they do not directly show how much of the force contributes to ship propulsion. Therefore, the aerodynamic force was resolved into thrust and side-force components. This allowed the influence of sail orientation and AWA to be evaluated in terms of useful forward force and the side loading imposed on the vessel. In this way, the analysis shows that the most suitable operating condition is not necessarily the one with the highest lift, but the one that provides a good balance between thrust generation and reasonable side force.

The configurations with the highest lift are not necessarily the best configuration for the ship's propulsion. A large lift force may also produce large side forces or drag depending on the apparent wind direction. Hence, the aerodynamic performance of the rigid wingsail must be understood in terms of wind-force components such as lift and drag, as well as ship-based components such as thrust and side force. This has also been described in detail in section 4.3.

2.4 High Lift Device and Flow Control

High-lift devices are artificial or additional enhancements implemented to improve the lift force of an airfoil, Ahmed et al. (2013). In the aviation sector, these devices are used during take-off and landing, where high lift is required at relatively low speeds. In maritime wind propulsion, the same principle applies: increasing the aerodynamic forces produced by the wingsail can improve thrust over a wide range of AWAs, as discussed in the previous section. High-lift devices are commonly categorized by their position on the airfoil, such as LE and TE devices, Arra et al. (2021).

A common type of LE device is a slat, which is an auxiliary element placed near the LE of the airfoil. The main purpose is to increase the maximum C_L and delay the stall by allowing the airfoil to operate at higher AoA before any large flow separation occurs, van Dam (2002). The slats work by modifying the pressure distribution and reducing the adverse pressure gradient on the suction side. It helps the BL attach over a longer distance on the airfoil surface, delaying flow separation and allowing the lifting surface to remain effective at higher angles of the incoming flow, Li and Yang (2016).

The TE flaps are also an important type of high-lift device, commonly used to modify

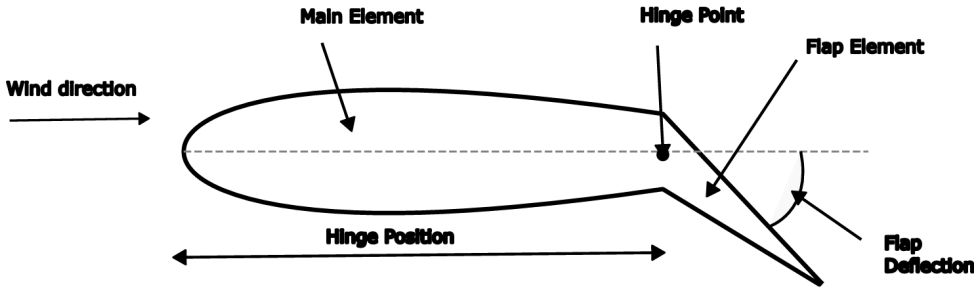

Figure 6: Hinged Flap Geometry of the airfoil

airfoil and wingsail performance. When the flap is deflected, it increases the airfoil's effective camber and changes the pressure distribution. Hence, the airfoil with a TE flap generates higher lift than the plain, undeflected flap airfoil at the same AoA. Different types of flaps are used depending on the required aerodynamic performance and design complexity, including plain, slotted, and hinged flaps, Ahmed et al. (2013).

Other high-lift devices use flow control methods. A flow control refers to techniques that are used to modify the flow field to improve the aerodynamic performances, such as an increase in lift, drag reduction, and delay BL separation, Ali et al. (2018). They are commonly divided as active and passive flow control depending upon the external energy input required. Active flow control requires an external energy input, such as suction, blowing, or synthetic jet actuation. Passive flow control does not require continuous external energy input; instead, it relies on geometric modifications such as slats, flaps, vortex generators, or multi-element configurations.

Multi-element airfoils use two or more aerodynamic elements separated by a slot or gap. The interaction between these elements can improve lift generation by allowing the downstream element to operate with a more favourable pressure distribution and a refreshed boundary layer. The slot between the elements can delay separation and increase the maximum lift, although the aerodynamic benefit depends strongly on the gap size and position. If the gap is not suitable, viscous losses and wake interaction can increase drag and reduce the overall aerodynamic efficiency ,van Dam (2002).

For the present thesis, the most relevant high-lift concept is the hinged trailing-edge flap (see Figure 6). Hinged flaps provide a relatively simple way to modify the effective camber of a rigid wingsail section without requiring a more complex multi-element

mechanism or active flow-control system. By changing the flap deflection angle and hinge position, the pressure distribution, lift generation, drag penalty, and flow-separation behaviour can be altered. Therefore, hinged-flap configurations are suitable for investigating how geometric changes affect the aerodynamic performance of a wingsail airfoil.

2.5 Research Gap

Previous studies like Fang et al. (2024), Von Klemperer et al. (2023),Jiang et al. (2024), etc have shown that the rigid wingsails, hinged flaps, and multi-element airfoils can improve the aerodynamic performance for the WASP. However, performance depends strongly on the selected geometry, flap configuration, apparent wind direction, gap element spacing, and other factors. For the ship propulsion, a high lift coefficient is not sufficient by itself because the useful aerodynamic thrust acting in the ship's direction is critical. Therefore, the present thesis discusses about the research objectives which were presented in the Research objectives.

Several studies have investigated the effect of the TE flaps, articulated profiles, and modifications of the camber. Ahmed et al. (2013) studied the flapped NACA 0012 airfoil using a two-dimensional CFD setup with SST k-ω turbulence model, which showed that the deflection of the flaps changed the lift and drag behavior. In Obeid et al. (2017) investigated a NACA 0015 airfoil with a 30% TE flap. The results showed that increasing flap deflection increased the maximum lift coefficient and adjusted the zero-lift AoA to negative angles; despite this fact, it reduced the stall angle. The reported maximum lift coefficient was around 2.2 at flap deflection of 50°. Fatahian et al. (2020) studied the flap airfoil at $Re = 5 \times 10^5$ with flap deflection of 15° with hinge positions considered as 0.7c to 0.9c. The results showed that the hinge position influenced the performance, with the lift coefficient increasing as the hinge moved closer to the TE. They also showed the suction flow control may increase the lift-to-drag ratio by approximately 35.8% for the perpendicular suction and 25% for the tangential suction at 12° AoA and hinge position of 0.9C. Kamliya Jawahar et al. (2018) showed experimental and numerical results that the morphing TE camber profiles can affect the lift, drag, pressure distribution, and wake development. The results indicated that cambered flap profiles produce more lift than moderate-cambered profiles. In the context of WASP, Jiang et al. (2024) studied a foldable three-element wingsail using the unsteady RANS with SST k-ω. The results showed that

a concave wingsail configuration produced higher lift, lower drag, and stable surface flow than a plain wingsail. At an AoA of 8°, the concave configuration produced a thrust coefficient approximately 23.5% higher than the plain wingsail configuration. Ding et al. (2025) investigated a rigid wing-tail sail configuration using the NACA 0020 as the main sail and a NACA 0018 as the tail sail. The tail sail area varied from 25% to 40% of the main sail area and considered tail deflection angles from 0° to 15° over the AoA 0° to 30°. The results showed that the hybrid wingtail system achieved the maximum lift coefficient of 29.5% higher than the single wingsail and an 11.6% improvement over the slotted flap sails.

Ma et al. (2025) studied the isolated, tandem, and parallel double wingsail arrangements and showed that AWA influences the aerodynamic interference. The isolated wingsails experienced a 57% thrust coefficient loss at an AWA of 180° while parallel double wingsails showed a 39% thrust coefficient reduction at 100°. They also reported that the spacing to chord ratio of 3.33 improved the mean thrust coefficient by 2.7% for the tandem wingsails and 6.5% for the parallel wingsails. Wang et al. (2024) studied the two-element wingsail arrangements at relative wind angles of 30°, 90°, 120°. The results indicated that the minimum horizontal spacing between the wingsails should be about 1.5c while an optimum arrangement was obtained with a horizontal spacing of 4c and longitudinal spacing of 10c. Lee et al. (2016) optimized multiple wingsails arranged in a single row by considering the flap length, deflection angle, AoA, and wind directions of 45°, 90°, 135°. Their optimizations improved the average thrust performance compared with the baseline configurations.

The gap between the main element and the flap of the multi-element airfoil affects the pressure distribution, BL development, and flow separation on the downstream element van Dam (2002). Cvetelina Velkova et al. (2015) studied the gap sizes of 1.8%c, 2.8%c for the NACA 2412 airfoil. The results showed that changing the gap between the main airfoil element and the flap element can influence the lift and drag behaviour. Kuang et al. (2023) where a two-element wingsail was studied and reported that the chord length ratio between the front and rear sails increased in lift and thrust. The optimal chord length ratio was around the range of $c1/c2$ of 1.5 to 3, but it was also observed that the smaller chord ratios and larger sail deflection angles lead to unstable flow.

2.5.1 Summary of the Research Gap

Overall, the reviewed studies show that hinged flaps, AWA, and gap spacing influence the aerodynamic performance of wingsails and multi-element airfoils. Previous work reports improvements in lift, thrust, or aerodynamic efficiency using articulated wingsails, flap deflection, multi-element arrangements, and optimized spacing between aerodynamic elements. However, these studies are not directly comparable because they use different airfoil sections, Reynolds numbers, turbulence models, geometries, and performance measures. Some focus mainly on aircraft-type high-lift systems, while others examine complete wingsail arrangements or multiple-sail interactions on ships.

A further limitation is that many studies do not combine the effects of hinge position, flap deflection, apparent wind direction, and gap size within a single consistent CFD framework. Several studies focus mainly on lift improvement, although high lift alone is not sufficient for ship propulsion. For a wingsail on a ship, the aerodynamic force must also be resolved into thrust and side-force components relative to the ship's direction. Therefore, a configuration with a high lift coefficient may still be less useful if it produces high drag or an unfavorable thrust component.

Another gap is that many previous works are based either on simplified two-dimensional airfoil studies or on complete three-dimensional wingsail arrangements. However, direct comparison between these studies is difficult because they often use different geometries, Reynolds numbers, turbulence models, and performance measures. In particular, the combined influence of hinge position, flap deflection, and gap size on lift, drag, thrust-related forces, and local flow behaviour has not been fully addressed for the NACA 0018-based wingsail configuration considered in this thesis.

Therefore, a controlled CFD study is needed to compare these geometric parameters using the same numerical setup. In this thesis, a two-dimensional approach is used to isolate the aerodynamic effects of hinge position, flap deflection, and gap size before introducing the additional complexity of three-dimensional effects and full-ship installation. The results should therefore be interpreted as sectional aerodynamic trends, while three-dimensional and ship-level effects remain important topics for future work.

This thesis is motivated by this gap. It uses a common OpenFOAM-based CFD workflow to compare selected hinged-flap and gap configurations for a NACA 0018-based rigid wingsail airfoil. It evaluates not only lift and drag, but also thrust-related force and

selected pressure and velocity fields. In this way, the thesis provides a consistent aerodynamic comparison of the main parameters that affect the performance of a simplified rigid wingsail section for wind-assisted ship propulsion. These are discussed in detail in the methods and results sections.

3 Methods

3.1 Physical Modelling and Solution approach

The numerical simulations in this thesis were performed to investigate the aerodynamic behaviour of NACA 0018-based rigid wingsails. The main purpose of the simulations was to compare how different geometric parameters influence the aerodynamic force coefficients and the surrounding flow field. The flow has been considered Newtonian, incompressible, and turbulent, with constant fluid properties. These assumptions are appropriate for the present low-speed simulations because the inlet velocity was sufficiently low for compressibility effects to be neglected.

The simulations were carried out using a steady Reynolds Averaged Navier Stokes (RANS) model. In this approach, the mean flow field is solved, while the effects of turbulence are represented by using turbulence modelling. RANS modelling was selected because the study involved a relatively large number of cases, including hinge positions, flap deflections and gap configurations. Compared to LES or DNS, a steady RANS approach provides a practical balance between computational cost and aerodynamic trends for the CFD study.

The SST k–ω model was used for the RANS simulations. It was selected because the flow around the airfoil and flap configurations is wall-bounded and can involve adverse pressure gradients and flow separation. These effects, which are important near the TE and flap region, strongly influence the lift and drag coefficients. It is suitable for the external aerodynamic flow because it combines the near-wall behaviour of the k–ω model with the freestream robustness of the k–ϵ. This makes the SST k–ω well suited than the simple two-equation turbulence models for the cases where the separation may occur. Hence, it was suitable for comparing the aerodynamic trends of the plain, hinged flap and gap configurations.

These simulations were carried out in the OpenFOAM software using the steady incompressible solver `simpleFoam`. This solver is based on the finite volume (FV) method and uses the SIMPLE pressure-velocity coupling algorithm. The steady RANS approach was used because the study required many simulations for different angles of attack and geometric configurations. This made LES less practical within the available project time, as it would have required much higher computational resources. Therefore, steady RANS

was considered suitable for comparing the main aerodynamic trends between the different cases.

A two-dimensional approach was used to reduce computational cost and enable testing of many other configurations within the available project time. This simplification is suitable for comparing the relative aerodynamic trends between the flap configurations. However, it also introduced a limitation that three-dimensional flow structures, unsteady vortex shedding and detailed post-stall behaviour cannot be fully captured using the steady two-dimensional RANS simulations. Therefore, the results are to be interpreted as a comparison of the aerodynamic trends rather than exact wingsail performance predictions.

3.2 Geometry Definition

The reference geometry used in this study was the NACA 0018 airfoil. This airfoil was selected because it is symmetric, well-documented, and sufficiently thick to represent a simplified rigid wingsail section. The symmetric profile is relevant for wingsail applications because the apparent wind may approach the sail from either side. The 18% thickness also provides a simple representation of a rigid profile with sufficient structural thickness.

The airfoil coordinates were obtained from the AirfoilTools database for the NACA 0018 airfoil AirfoilTools (2026). Approximately 180 coordinate points were used to describe the airfoil surface with sufficient geometric smoothness. These coordinates were imported into FreeCAD, where the airfoil geometry was reconstructed and prepared for export as an STL surface for meshing in OpenFOAM. The geometry was scaled so that the chord length was $c = 1\,\mathrm{m}$. This chord length was used as the reference length for the aerodynamic coefficient calculations.

Before meshing, the geometry was checked for alignment and positioning. The airfoil was oriented with the leading edge facing upstream and the trailing edge facing downstream. This check was performed to prevent incorrect orientation or geometric offsets before generating the computational mesh.

The angle of attack was implemented by rotating the STL geometry relative to the fixed incoming flow direction. Therefore, the free-stream velocity direction was kept constant, while the airfoil geometry was rotated and remeshed for each angle of attack. The validation cases were simulated for angles of attack from 0° to 20°, using increments of

5°. Negative angles of attack were not included for the baseline NACA 0018 airfoil because the profile is symmetric. Therefore, the corresponding force behaviour is expected to be symmetric apart from the sign convention for lift.

3.3 Computational Domain and Boundary Conditions

The figure 7 shows that the computational domain was defined around the airfoil, with the airfoil positioned near its centre. The domain was chosen to be sufficiently large so that the far-field boundaries did not significantly influence the near-airfoil flow field. In the present setup, the domain extended from $-24c$ to $24c$ in the streamwise direction and from $-24c$ to $24c$ in the transverse direction. Since the chord length was $c = 1\,\mathrm{m}$, this corresponds to a domain size of $48\,\mathrm{m} \times 48\,\mathrm{m}$. The spanwise thickness of the two-dimensional domain was $0.05\,\mathrm{m}$.

A constant free-stream velocity of $U_\infty = 10\,\mathrm{m/s}$ was used for all validation cases. This velocity was selected as a representative low-speed inflow condition for the wingsail airfoil study. At this speed, compressibility effects were negligible, so the flow was treated as incompressible. The air density was set to $\rho = 1\,\mathrm{kg/m^3}$.

The computational domain consisted of the patches `inlet`, `outlet`, `topAndBottom`, `wing`, `front`, and `back`. The `inlet` patch was used to prescribe the incoming free-stream velocity, while the `outlet` patch allowed the flow to leave the domain. The `wing` patch represented the airfoil surface and was treated as a no-slip wall. The `front` and `back` patches were treated as `empty` boundaries so that the simulation could be solved as a two-dimensional case.

The initial turbulence quantities were estimated from standard inlet turbulence relations for the k–ω model. The freestream velocity was $U_\infty = 10$ m/s and the Reynolds number was approximately $Re = 200000$, based on a chord length of $c = 1$ m. Therefore, the kinematic viscosity used for the validation case was

$$\nu = \frac{U_\infty c}{Re} = \frac{10 \times 1}{200000} = 5.0 \times 10^{-5}\ \mathrm{m^2/s}.$$

A turbulence intensity of $Tu = 5\%$ was used. The turbulent kinetic energy was calculated as

$$k = \frac{3}{2}(U_\infty Tu)^2,$$

which gives

$$k = \frac{3}{2}(10 \times 0.05)^2 = 0.375 \text{ m}^2/\text{s}^2.$$

The specific turbulence dissipation rate was estimated using the eddy-viscosity relation

$$\omega = \frac{k}{\nu(\mu_t/\mu)}.$$

Using an eddy viscosity ratio of $\mu_t/\mu = 1225$, this gives

$$\omega = \frac{0.375}{(5.0 \times 10^{-5})(1225)} \approx 6.123 \text{ s}^{-1}.$$

Therefore, the inlet turbulence quantities used for the validation simulations were $k = 0.375$ m^2/s^2 and $\omega = 6.123$ s^{-1}. These values were kept constant for the validation cases so that the effect of changing AoA could be compared under consistent inflow turbulence conditions.

Table 1: Boundary conditions used for the two-dimensional airfoil simulations.

Patch	Field	Boundary condition
`inlet`	U	fixedValue
`inlet`	p	zeroGradient
`outlet`	U	zeroGradient
`outlet`	p	fixedValue
`topAndBottom`	U, p	far-field/slip-type condition
`wing`	U	noSlip
`wing`	p	zeroGradient
`front`, `back`	all fields	empty

The wing surface was modelled as a solid wall. For the velocity field, a `noSlip` boundary condition was applied on the wing surface, while a zero-gradient pressure condition was used for the pressure field (OpenCFD Ltd., 2023a). In addition to the velocity and pressure boundary conditions shown in Table 1, near-wall turbulence treatment was applied using OpenFOAM wall-function boundary conditions (OpenCFD Ltd., 2023c). The turbulent viscosity was specified using `nutkWallFunction`, the turbulent kinetic en-

ergy using `kqRWallFunction`, and the specific dissipation rate using `omegaWallFunction`. The `nutkWallFunction` boundary condition is documented as a turbulent-viscosity wall function based on turbulent kinetic energy (OpenCFD Ltd., 2023b). These boundary conditions were identified directly from the OpenFOAM case files `0/U`, `0/p`, `0/k`, `0/nut`, and `0/omega`.

3.4 Mesh Generation

The computational mesh was generated using the OpenFOAM utilities `blockMesh` and `snappyHexMesh`. First, `blockMesh` was used to create the structured background mesh and to define the far-field computational domain. This background mesh provided the domain discretisation before the airfoil geometry was introduced.

After the background mesh was generated, the NACA 0018 STL surface was imported into the computational domain. The mesh was then refined locally using `snappyHexMesh`. Local refinement was applied around the airfoil surface and in the downstream wake region. The refinement near the airfoil was used to improve the resolution of pressure and velocity gradients near the wall, while the wake refinement was used to better capture downstream flow behaviour.

The far-field region was kept relatively coarse in order to reduce the total number of cells. This was considered suitable because the highest mesh resolution was mainly required near the airfoil surface and in the wake, where the strongest velocity and pressure changes occur. This refinement strategy allowed the important flow regions to be resolved without unnecessarily increasing the cell count throughout the entire domain.

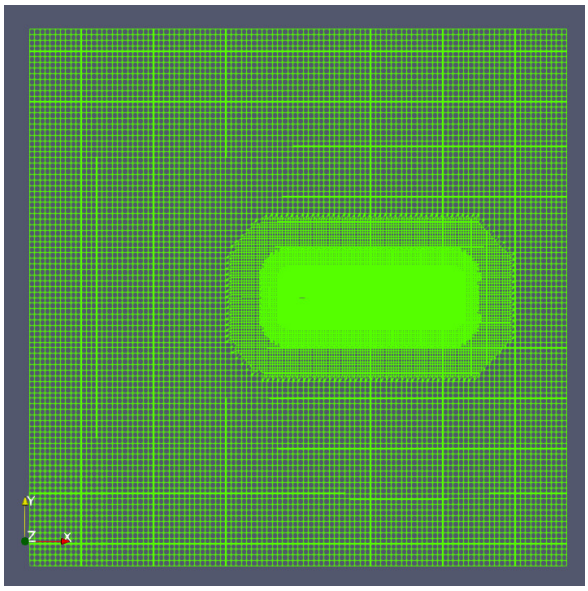

(a) Overall computational domain.

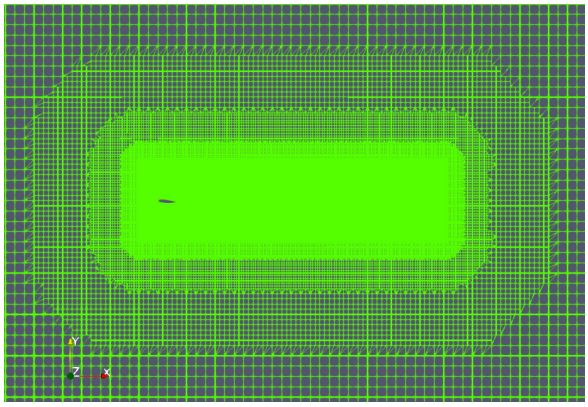

(b) Refined mesh in the downstream wake region.

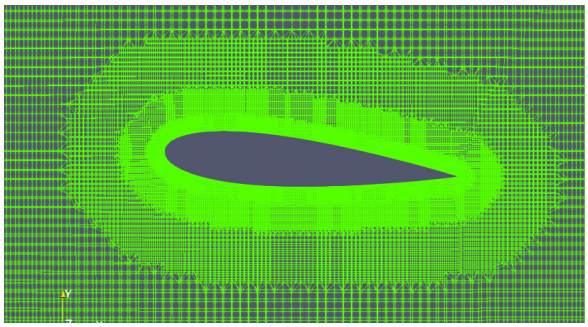

(c) Local mesh refinement around the airfoil.

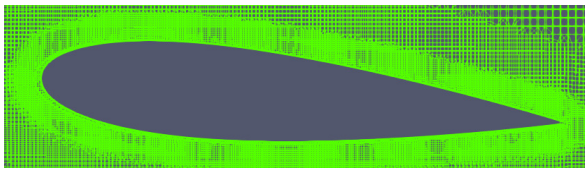

(d) Near-airfoil mesh resolution.

Figure 7: Computational mesh used for the airfoil simulations, showing the global domain and local refinement regions.

Figure 7 shows the computational mesh used for the airfoil simulations. The full-domain view shows the position of the airfoil inside the far-field domain, while the closer views show the refinement around the airfoil and in the downstream wake region. The refinement was concentrated in these regions because the strongest pressure and velocity gradients occur close to the airfoil surface and in the wake. The far-field region was kept relatively coarse to avoid unnecessary increases in the total cell count.

3.5 Mesh Independence Study

The mesh independence study was carried out to ensure that the aerodynamic coefficients were independent of mesh resolution. The study was performed for the plain NACA 0018 airfoil at an AoA of 5°, using the same computational domain, boundary conditions, solver

settings, etc., which have been discussed in 3.3. The AoA of 5° was selected because the flow is attached still, and the aerodynamic coefficients are expected to be sufficiently steady for comparing the effect of the mesh refinement.

There were four mesh resolutions, which were tested, and the refinement level is denoted by **resf**, which is a mesh refinement factor used in the meshing script. These values are specific to the present OpenFOAM setup; the mesh comparison is mainly interpreted using the total number of cells N_{cell} instead of **resf** itself. Increasing the **resf** increased the total number of cells from 26,739 cells for the coarsest mesh to 165,844 cells for the finest mesh.

Table 2: Mesh independence study for the plain NACA 0018 airfoil at $\alpha = 5°$.

resf	N_{cells}	F_x	F_y	C_L	C_D	y^+_{avg}	ΔC_L	ΔC_D	y^+_{min}	y^+_{max}
2	26739	8.99×10^{-2}	1.1922	0.47688	3.60×10^{-2}	13.2805	–	–	4.74319	85.171
3	59726	3.69×10^{-2}	1.2900	0.51648	1.477×10^{-2}	13.6800	0.03960	-2.12×10^{-2}	3.47060	96.1778
4	106771	3.70×10^{-2}	1.2613	0.50452	1.48016×10^{-2}	13.7900	-0.01196	3.16×10^{-5}	4.94670	69.1778
5	165844	3.70×10^{-2}	1.256272	0.5025088	1.48×10^{-2}	13.9193	-0.0020112	-4.00×10^{-6}	4.38025	44.468

Table 2 is used to summarize the mesh independence results. This indicated that the lowest mesh resolution was insufficient to resolve the near-wall flow and its development. As the mesh was refined, both the lift and drag coefficients became less sensitive to increases in the number of cells. The large change occurred between the two coarse meshes, while the difference between the two finest meshes was small. The numerical solution should gradually converge to a mesh-independent value as the grid resolution is increased. The drag coefficient was sensitive to the coarsest mesh because drag depends strongly on near-wall gradients, pressure distribution, and wake resolution.

The y^+ values were checked in order to evaluate the near-wall mesh resolution. The average y^+ values were almost in a similar range for the meshes, while the maximum y^+ values reduced for the finer meshes. Additionally, the y^+ values depended on the local wall shear stress, which varied as the flow changed with the refined mesh. Hence, y^+ should be understood as an implication of consistent near-wall treatment rather than of the mesh-refinement trend near the airfoil.

Figure 8 shows the variation of C_L with the number of cells. The lift coefficient differs between the coarsest and intermediate meshes, indicating that the coarse mesh was not refined sufficiently to yield mesh-independent lift variations. By further refining the mesh, the variation of C_L became more smaller and it implied that the lift became less dependent

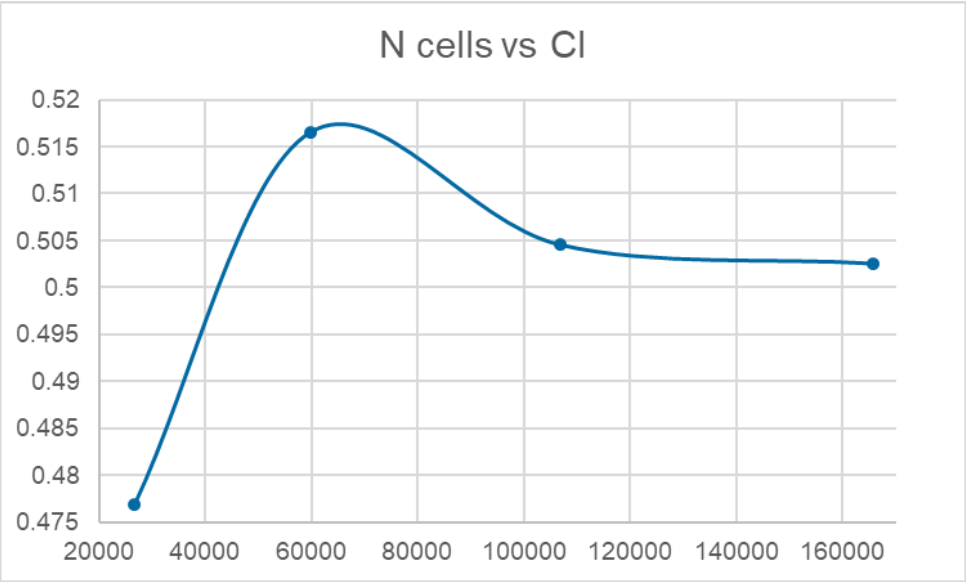

Figure 8: Comparison of Number of cells vs C_L

on the mesh resolution as the number of cell increases.

Figure 9 shows that the drag coefficient varies with the number of cells and is more sensitive to the coarse mesh than the lift coefficient. It is because the drag prediction depends strongly on the near-wall velocity gradients, pressure distribution, and wake resolution. The coarsest mesh gives a very varied drag value, while the finer meshes produce very similar C_D values. The drag became almost flat, indicating that the drag prediction became mesh-independent for the finer mesh. The C_L and C_D trend discussed here showed that the values changes at the low mesh resolution but becomes almost constant when the mesh is refined more then $resf = 4$. Therefore, $resf = 4$ was chosen, as it yielded force coefficients closer to those of the finer mesh while avoiding the higher computational cost and time required by $resf = 5$.

3.6 Numerical Setup

The simulations were carried out using the steady incompressible OpenFOAM solver `simpleFoam`. This solver was selected because the aim of the simulations was to obtain converged mean aerodynamic coefficients for different angles of attack and geometric configurations, rather than to resolve unsteady flow fluctuations. Since the study included several validation and parametric cases, a steady solver was suitable, as it reduced computational cost while still allowing the main aerodynamic trends to be compared. Cases that did not reach acceptable convergence in the residuals and force histories were not

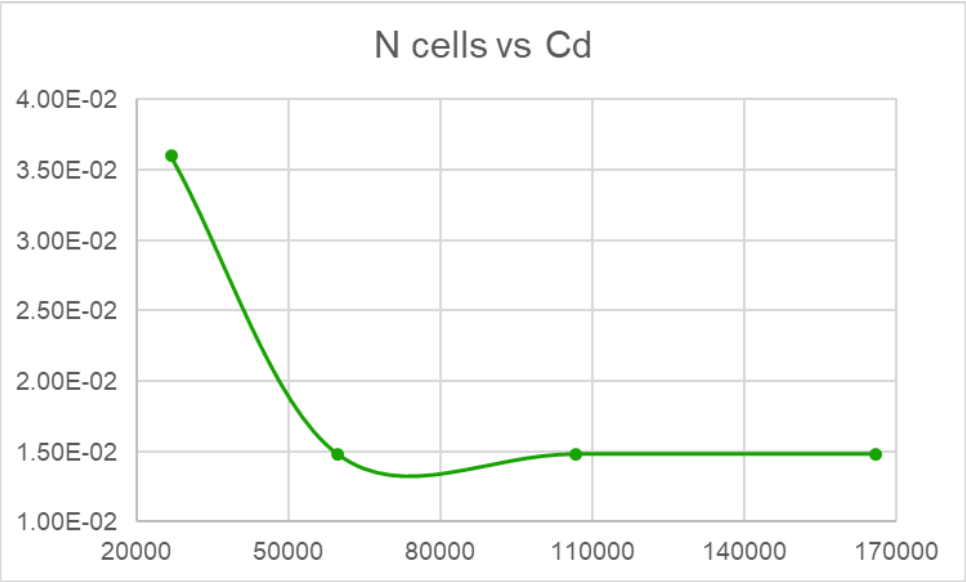

Figure 9: Comparison of Number of cells vs C_D

used for the final quantitative comparison.

The numerical settings were defined using the OpenFOAM dictionaries `controlDict`, `fvSolution`, and `fvSchemes`. In the steady-state framework, the simulation time was used as an iteration counter rather than as physical time. The simulations were run until the force coefficients reached steady behaviour or until a maximum of 30,000 iterations was reached. The results were recorded every 100 iterations to monitor solution development during the run. The aerodynamic forces were extracted using the OpenFOAM force function object.

Pressure–velocity coupling was handled using the SIMPLE algorithm. Two non-orthogonal correctors were used in the pressure correction procedure. This was included because the locally refined mesh may contain non-orthogonal cells, especially near the airfoil surface and refinement regions. The correction improved the robustness of the pressure solution on the adopted mesh.

The pressure equation was solved using the GAMG solver. The velocity equation and the turbulence transport equations for turbulent kinetic energy and specific dissipation rate were solved using `smoothSolver` with Gauss–Seidel smoothing. Under-relaxation factors were applied to improve the stability of the iterative solution. A relaxation factor of 0.04 was used for pressure, while a value of 0.15 was used for velocity, turbulent kinetic energy, and specific dissipation rate. These low relaxation factors were used to reduce the risk of oscillations or divergence during the simulations.

The spatial discretisation schemes were defined in `fvSchemes`. Since the simulations were steady state, the time-derivative terms were set to `steadyState`. Gradient terms were discretised using a Gauss linear scheme. The convection term in the momentum equation was discretised using a bounded Gauss linear-upwind scheme based on the velocity gradient. The convection terms in the turbulence equations were discretised using bounded upwind schemes. Diffusion terms were discretised using a Gauss-linear-corrected scheme to account for mesh non-orthogonality. Linear interpolation and corrected surface-normal gradient schemes were also used.

The same numerical settings were used for the comparable validation and parametric cases. This ensured that differences in the aerodynamic coefficients were mainly due to changes in angle of attack or geometry, rather than to changes in the numerical setup.

3.7 Post-processing and Aerodynamic Coefficients

After the simulations were completed, the aerodynamic forces and moments acting on the airfoil were extracted using the OpenFOAM force function object. The total force was obtained from the pressure and viscous contributions acting on the airfoil surface. Since the free-stream velocity direction was fixed in the streamwise direction and the geometry was rotated to set the angle of attack, the force component in the x-direction was treated as drag, while the force component in the y-direction was treated as lift. The moment about the specified reference point was also extracted for the calculation of the moment coefficient.

The aerodynamic coefficients were calculated using the same reference quantities for all comparable cases. The airfoil chord length was $c = 1\,\mathrm{m}$, and the reference span used in the two-dimensional simulations was $b = 0.05\,\mathrm{m}$. This gave a reference area of

$$A_{\mathrm{ref}} = cb = 1 \times 0.05 = 0.05\,\mathrm{m}^2. \tag{5}$$

The air density was set to $\rho = 1\,\mathrm{kg/m^3}$, and the free-stream velocity was $U_\infty = 10\,\mathrm{m/s}$. Based on these values, the dynamic pressure was:-

$$q_\infty = \frac{1}{2}\rho U_\infty^2 = \frac{1}{2}(1)(10)^2 = 50\,\mathrm{N/m^2}. \tag{6}$$

Therefore, the denominator used for the lift and drag coefficient calculations was

$$q_\infty A_{\text{ref}} = 50 \times 0.05 = 2.5\,\text{N}. \tag{7}$$

The lift, drag, and moment coefficients were calculated using the definitions introduced in Equations 1–3. For all comparable cases, the same reference quantities were used. The airfoil chord length was $c = 1$ m, and the reference span used in the two-dimensional simulations was $b = 0.05$ m.

In the validation and hinged-flap studies, the main quantities used for comparison were the lift and drag coefficients. These coefficients were plotted against the AoA to assess how the airfoil and flap configurations influenced aerodynamic performance. The moment coefficient was also calculated where required, but the main discussion focused on lift and drag because these quantities directly describe the aerodynamic force behaviour of the wingsail section.

For the wingsail-orientation analysis, the lift and drag coefficients were transformed into thrust-related and lateral-force coefficients using the apparent wind angle relative to the ship direction. The thrust-related coefficient was used to estimate the useful forward force component, while the lateral-force coefficient represented the side-force component. These coefficients were calculated as

$$C_T = C_L \sin\beta - C_D \cos\beta, \tag{8}$$

$$C_S = C_L \cos\beta + C_D \sin\beta, \tag{9}$$

where β is the apparent wind angle relative to the ship direction. This post-processing step enabled the interpretation of the airfoil simulation results in the context of simplified wingsail propulsion.

Pressure and velocity contours were generated in ParaView to support the interpretation of the force-coefficient results. The velocity contours were used to observe wake development, acceleration around the airfoil, and possible regions of separated flow. The pressure contours were used to identify changes in pressure distribution around the airfoil and flap surfaces. For a fair comparison between cases, the same colour scale and camera view were used for similar configurations.

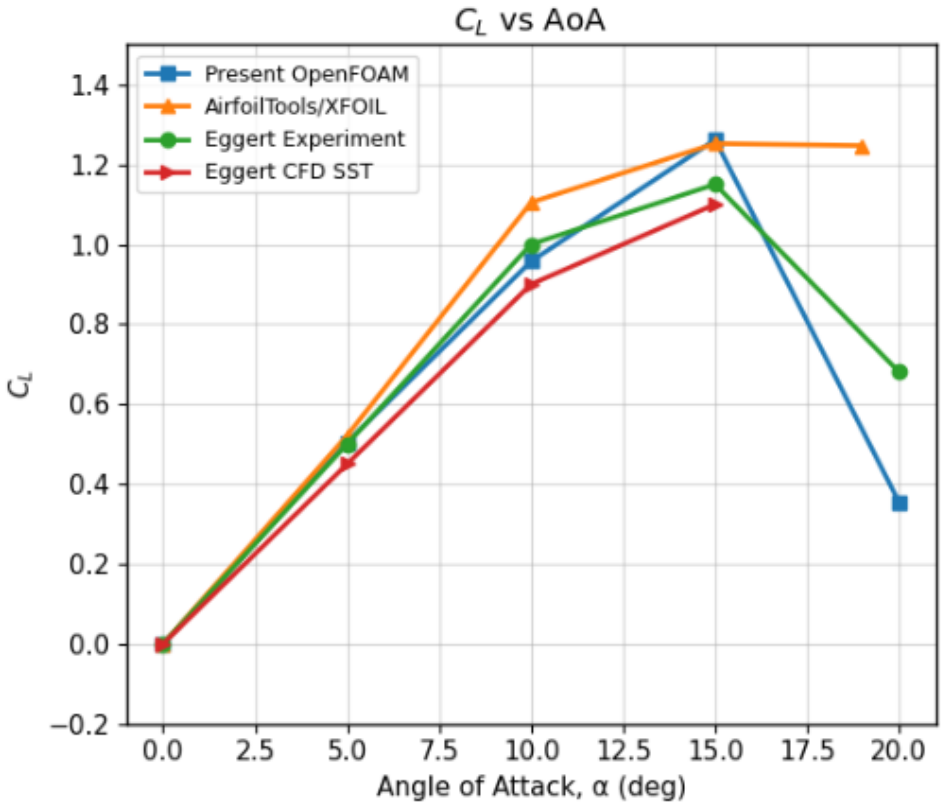

Figure 10: Comparison of C_L with AoA

4 Results

4.1 Validation Study

The validation study was carried out for the plain NACA 0018 before analysing the hinged-flaps and gap configurations. The purpose was to assess whether the OpenFOAM setup could reproduce the expected aerodynamic behaviour of a symmetric airfoil in the converged AoA range. The present result was compared with the reference data from Eggert and Rumsey (2017) and with the AirfoilTools polar dataset for the NACA 0018 airfoil. The AirfoilTools dataset used for the comparison was the XFOIL prediction polars for the NACA 0018 airfoil, specifically `(naca0018-il)` at a $Re = 200{,}000$, $N_{\text{crit}} = 9$, and $M = 0$ AirfoilTools (2026).The simulations were performed for the AoA from 0° to 20° in the increaments of 5°. The cases from 0° to 15° reached acceptable convergence and are used for the main quantitative comparison. The 20° case is retained, but it did not reach convergence and is therefore to be interpreted qualitatively only.

Figure 10 compares the lift coefficient C_L, which was obtained from OpenFOAM, with the reference data. At 0°, the present simulation gives C_L=0, which is expected for

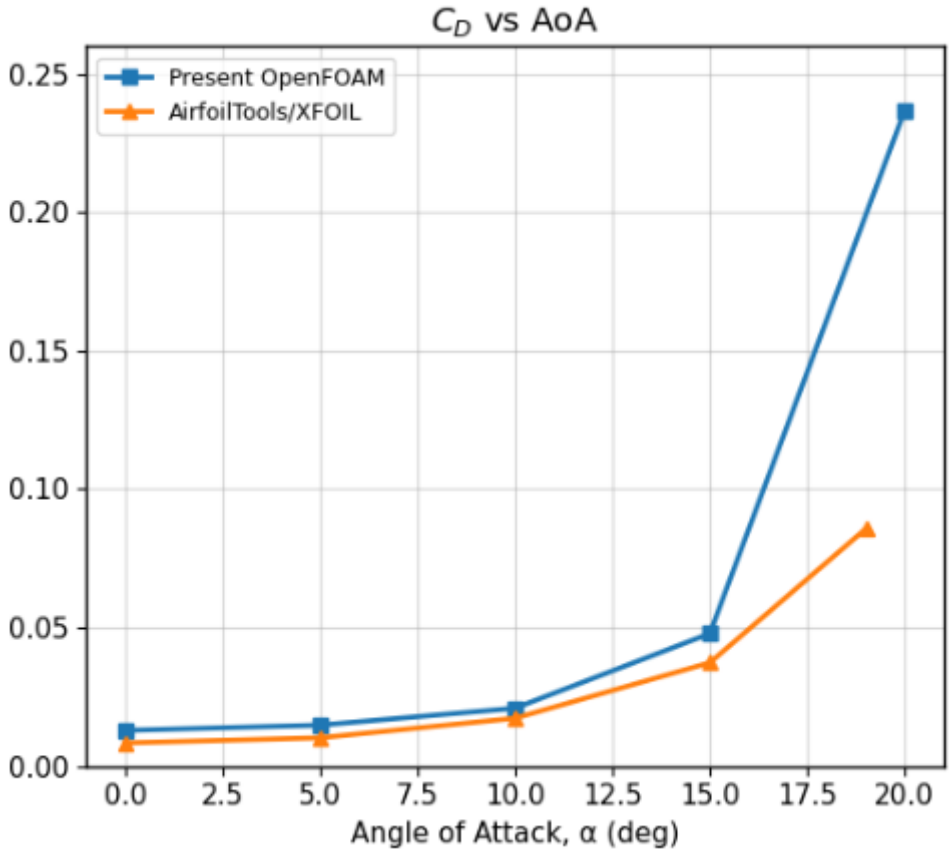

Figure 11: Comparison of C_D with AoA

a symmetric airfoil. From 5° to 15°, the lift coefficient increases from approximately 0.505 to 1.261. This follows the same trend observed in the Eggert and Rumsey (2017) reference data and the Airfoils Tools data. The results in this range indicate that the OpenFOAM setup captures the attached flow and pre-stall behaviour of the plain airfoil. At 20°, the lift coefficient decreases sharply to an approximate value of 0.354. However, the case was not converged; this value is not used as a valid quantitative validation point. Instead, it was used to indicate that the steady 2D RANS setup becomes unreliable when the airfoil enters a strong separated regime.

Figure 11 compares the drag coefficient C_D. In the converged range from 0° to 15°, the drag coefficient increases with AoA. The present OpenFOAM results gives C_D=0.0148 at 5°, C_D=0.0209 at 10°, and C_D=0.0479 at 15°. At 20°, the C_D increases sharply to approximately 0.237. This was included to show the behaviour of the solver at the high AoA, but should not be treated as a converged drag prediction. The large drag value is consistent with the development of a large separated wake.

The lift-to-drag ratio C_L/C_D in Figure 12 provides further indication of the airfoil's

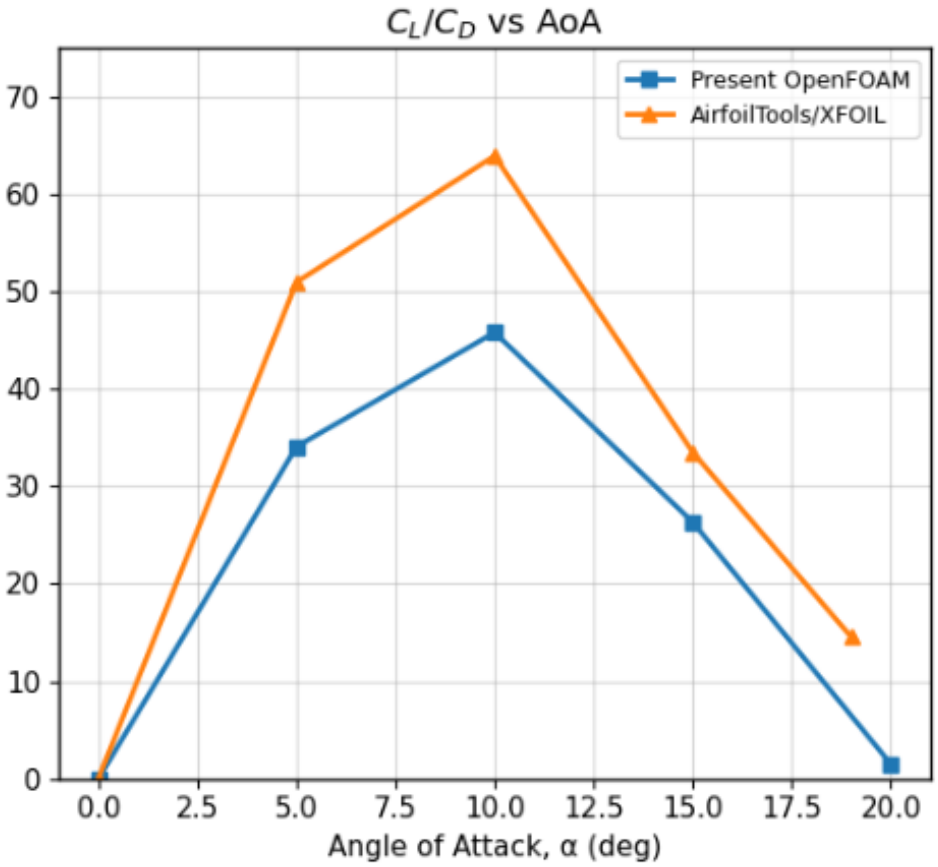

Figure 12: Comparison of C_L/C_D with AoA

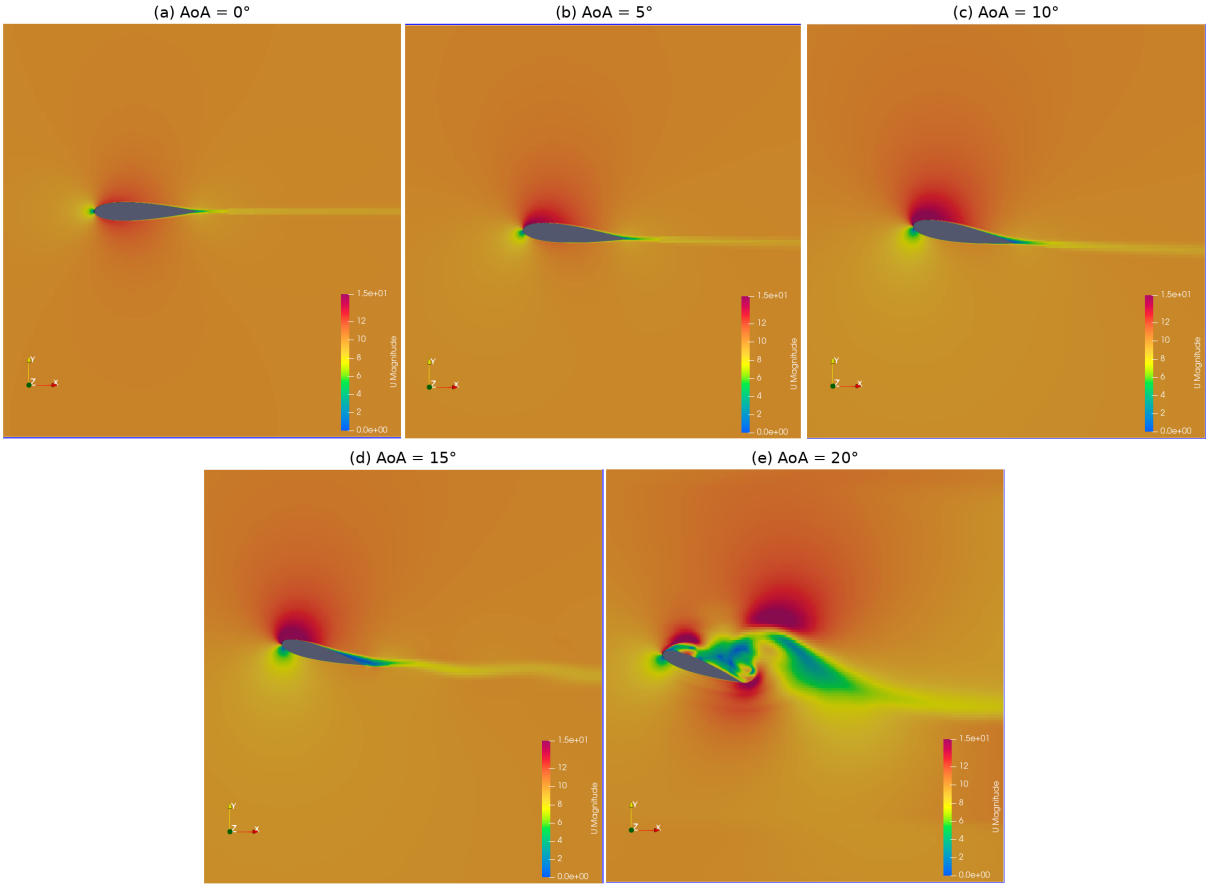

Figure 13: Velocity magnitude contours for the validation case at different AoA.

aerodynamic efficiency. In the present OpenFOAM results, the ratio increases from 34.1 at 5° to 45.8 at 10°, which shows that the airfoil becomes more aerodynamically efficient while the drag remains relatively low. After 10°, the ratio decreases to approximately 26.3 at 15°, even though the C_L continues to increase. At 20°, the ratio decreases sharply to approximately 1.5, consistent with a large increase in drag and a reduction in lift due to flow separation.

The velocity and pressure contours support the interpretation of the coefficient plots. At 0°, the pressure and velocity fields are almost symmetric, which corresponds to the near-zero lift coefficient. At 5° and 10°, the flows remain mostly attached, and the wake is narrow. At 15°, the wake becomes more visible, and the pressure difference across the airfoil is bigger, corresponding to the increase lift and drag. At 20°, the contours show a larger distributed wake effect and stronger flow separation behaviour. Overall, the validation shows that the OpenFOAM setup reproduces lift and drag trends of the plain NACA 0018 airfoil in the converged range from 0° to 15°. Therefore, the setup is suitable for comparing aerodynamic trends across the wingsail configurations in this thesis.

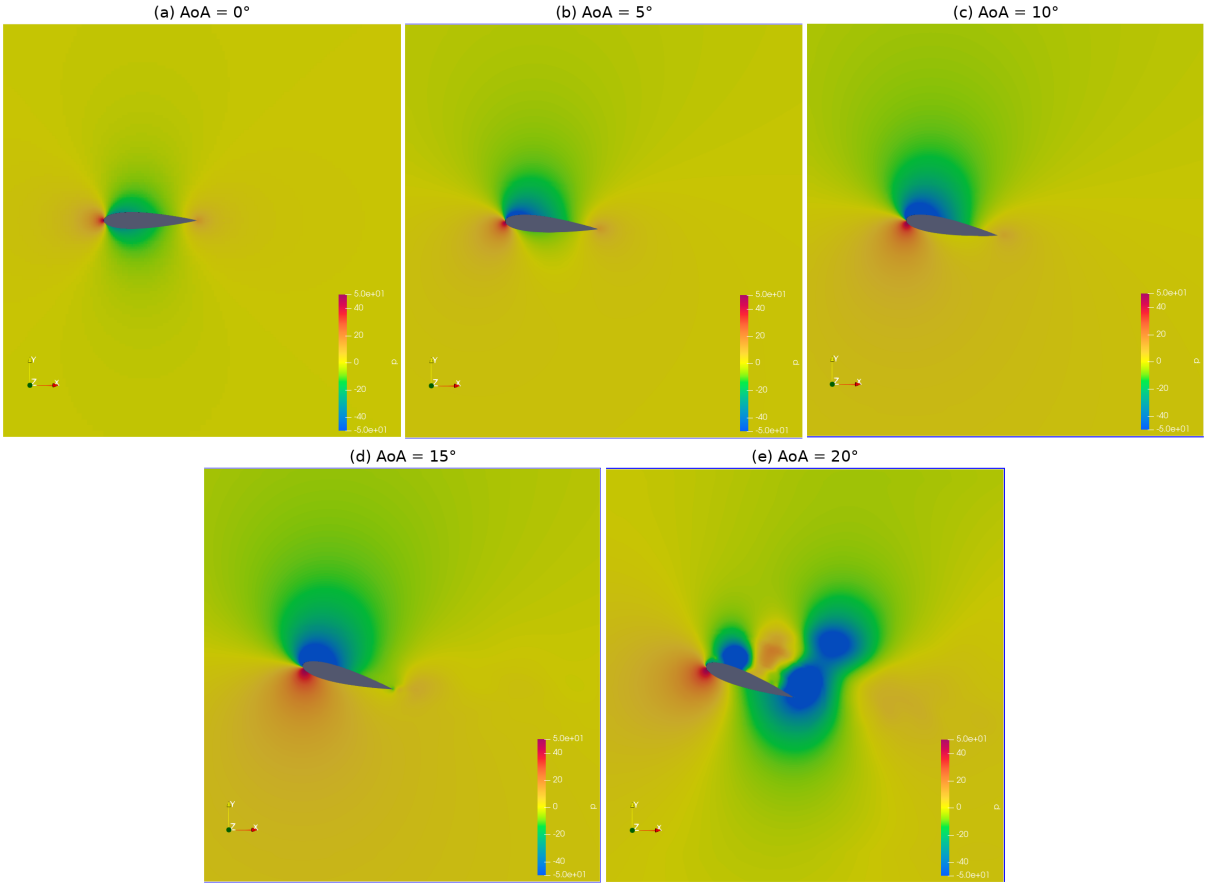

Figure 14: Pressure contours for the validation case at different AoA.

4.2 Hinged Flap Study

The hinged-flap study was conducted to examine how TE flap deflections and hinge position affect the aerodynamic performance of the NACA 0018 wing sail section. In this study, the hinged flap modifies the airfoil's effective camber. This changes the pressure distribution around the airfoil, thereby affecting the aerodynamic coefficients and promoting flow separation. The following subsections explain how the hinge position and flap angle configurations were implemented. The initial physical conditions and turbulent properties were kept constant, as in the validation study.

Table 3: Candidate hinge positions, flap deflections, and screening status in the hinged flap study

Hinge position (% chord)	**Flap deflection angles, δ (°)**	**Status**
40	0, 20, 40	Geometrically infeasible
50	0, 20, 40	Geometrically infeasible
60	0, 20, 40	Retained
65	0, 20, 40	Partially retained
70	0, 20, 40	Retained

Table 3 presents the hinge positions and flap deflection angles considered. It should be noted that the flap deflection angles were taken as only 3 variations to reduce computational time. In the following, 'HXX' denotes hinge position at XX% of the chord, 'DYY' flap deflection angle of YY°. For example, H70 represents a hinge located at x/c=0.7, and D20 represents the flap deflection of 20°. Several hinge positions and flap deflections were considered during the initial geometry screening. The hinge positions at 40% and 50% chords were excluded because the generated flap geometries were not suitable for the CFD study. These configurations produced poor geometry near the hinge region, leading to poor mesh quality and unreliable flow solutions. The flap deflections considered were 0°, 20°, and 40°. The zero-deflection case was geometrically identical across all hinge positions, since the flap is not rotated; hence, the D0 case was reported only once as a baseline configuration. The retained cases were H70D0, H70D20, H70D40, H60D20, H60D40 and H65D40. The H65D20 case was generated and meshed, but the solver did not converge on the force histories. Hence, the H65D20 case was excluded from the quantitative comparison.

Figure 15 shows the geometries for different flap deflection angles at a fixed hinge position of 70% of the chord. Increasing the flap deflection from 0° to 40° changes the TE

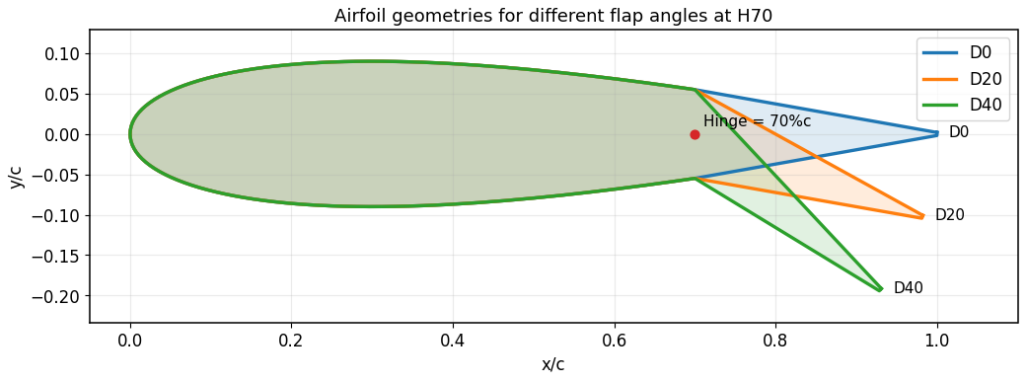

Figure 15: Airfoil geometries for different flap deflection angles at a fixed hinge position of 70% chord.

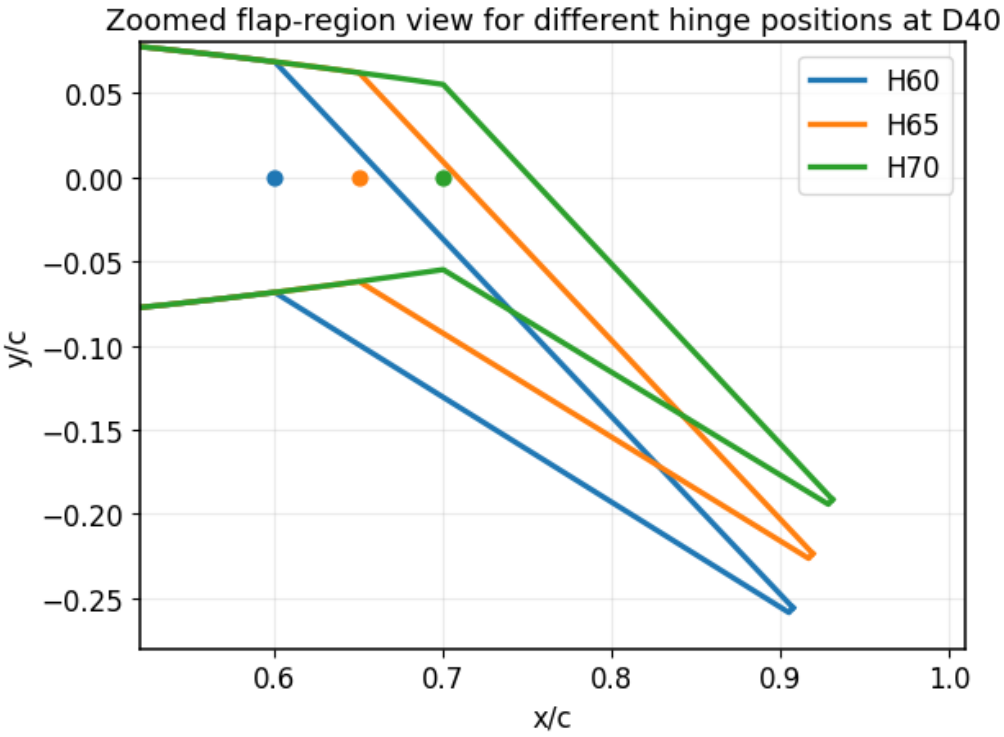

Figure 16: Zoomed flap-region view of airfoil geometries for different hinge positions at a fixed flap deflection of 40°.

section and increases the camber. The main airfoil element remains the same while the flap modifies the TE region. Figure 16 shows the effect of changing the hinge position at a fixed flap deflection of 40°. Moving the hinge position forward increases the length of the deflected flap, while moving the hinge rearward reduces the flap length.

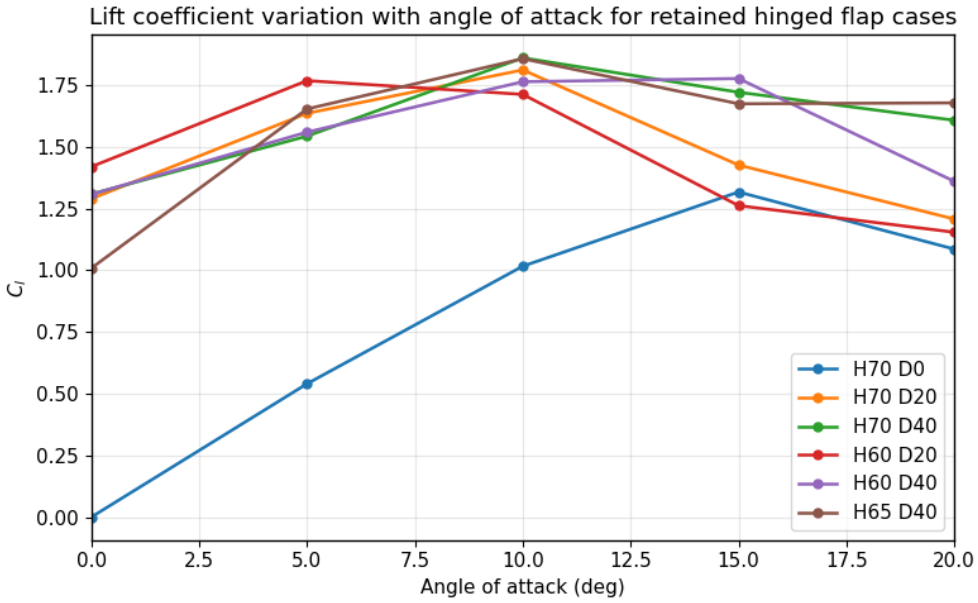

Figure 17: Lift coefficient variation with AoA for the retained hinged flap configurations.

Figure 17 shows the variation of the lift coefficient C_L with the AoA for the retained hinged flap configurations. The undeflected baseline case produces the lowest lift coefficient C_L over the AoA range. When the flap is deflected, the lift coefficient C_L increases because the effective camber of the airfoil is increased. This effect is clearly observed for both the 20° and 40° flap deflections. For H70 cases, increasing the flap deflection from 0° to 20° and then 40° produces clear increases in the lift coefficient C_L. This shows that flap deflection strongly affects the aerodynamic characteristics.

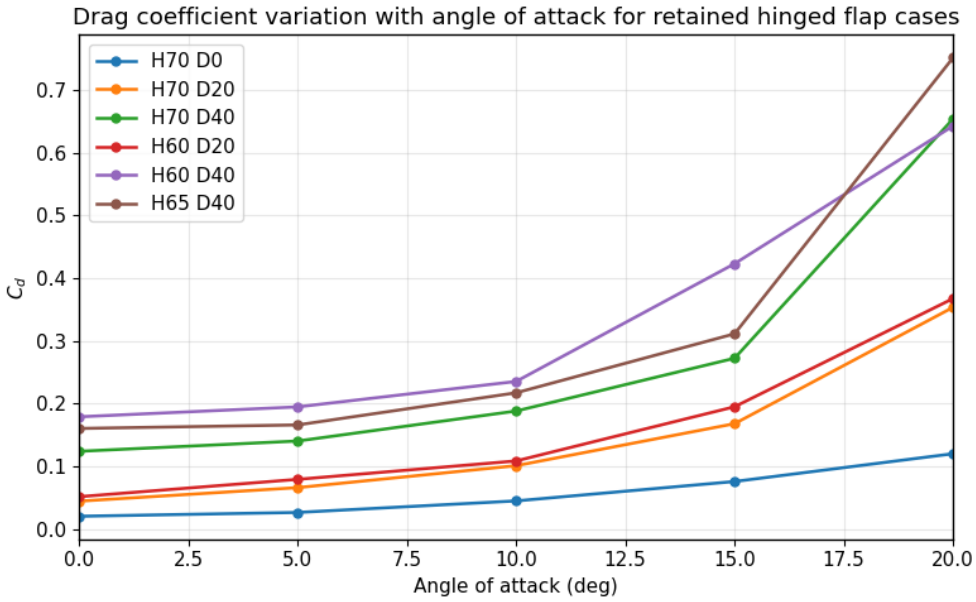

Figure 18: Drag coefficient variation with AoA for the retained hinged flap configurations.

However, this increase in lift is also accompanied by an increase in the drag as shown in Figure 18. The drag coefficient C_D increases with both the AoA and flap deflection. The H70D0 case has the lowest drag because there is no flap deflection and the airfoil remains closest to the plain NACA 0018 profile. The deflected cases produce higher drag because the flap increases the pressure difference and promotes stronger wake development near the airfoil's TE. The 40° flap deflection gives the largest drag values among the remaining H70 cases.

Compared to the flap deflections, the hinge position has less direct effects. Placing the hinge closer to the leading edge increases the length of the deflected flap and changes the TE camber distribution. For the 20° deflected cases, the H60 configuration produces higher lift at lower AoA than the H70. This nature is expected because the H60 has a longer deflected flap, which produces higher drag. At higher AoA, the influence of the hinge positions becomes less distinct because the flow is increasingly affected by the flow separation and development of the wake.

Figures 19 and 20 are the pressure and velocity contours for H60D20 and H70D20 at AoA of 10° used to examine the effect of the hinge position at the same flap deflection of 20°. The comparison shows the change of hinge locations and how it influences the flow field. The pressure contours show a clear pressure difference between the upper and lower surfaces in both configurations. For the H60D20, a larger portion of the TE is deflected because it is located further upstream. As a result, the pressure variation

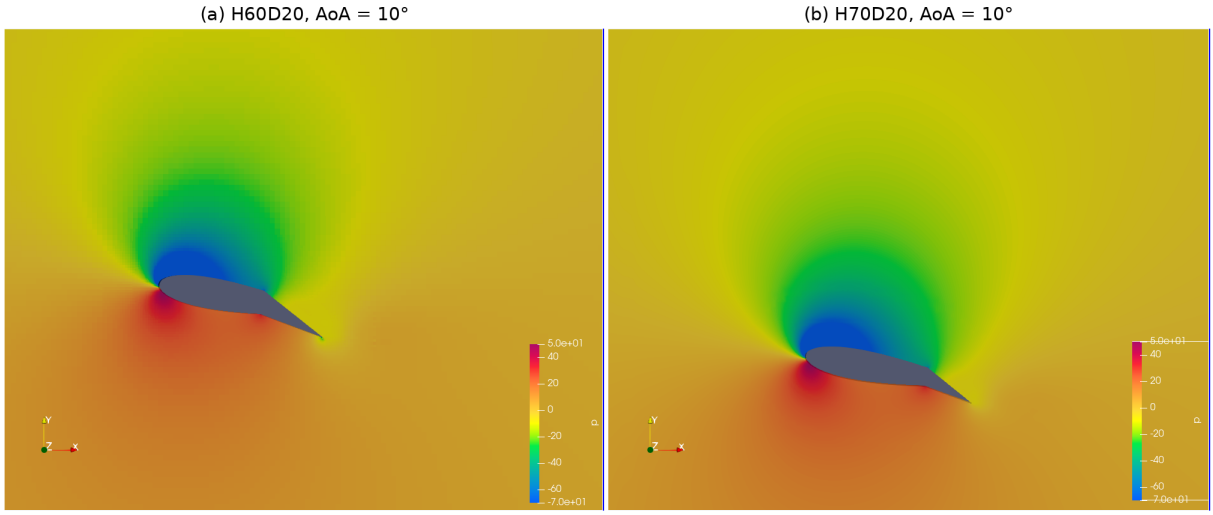

Figure 19: Pressure contour Comparison between H60D20 and H70D20 at AoA = 10°.

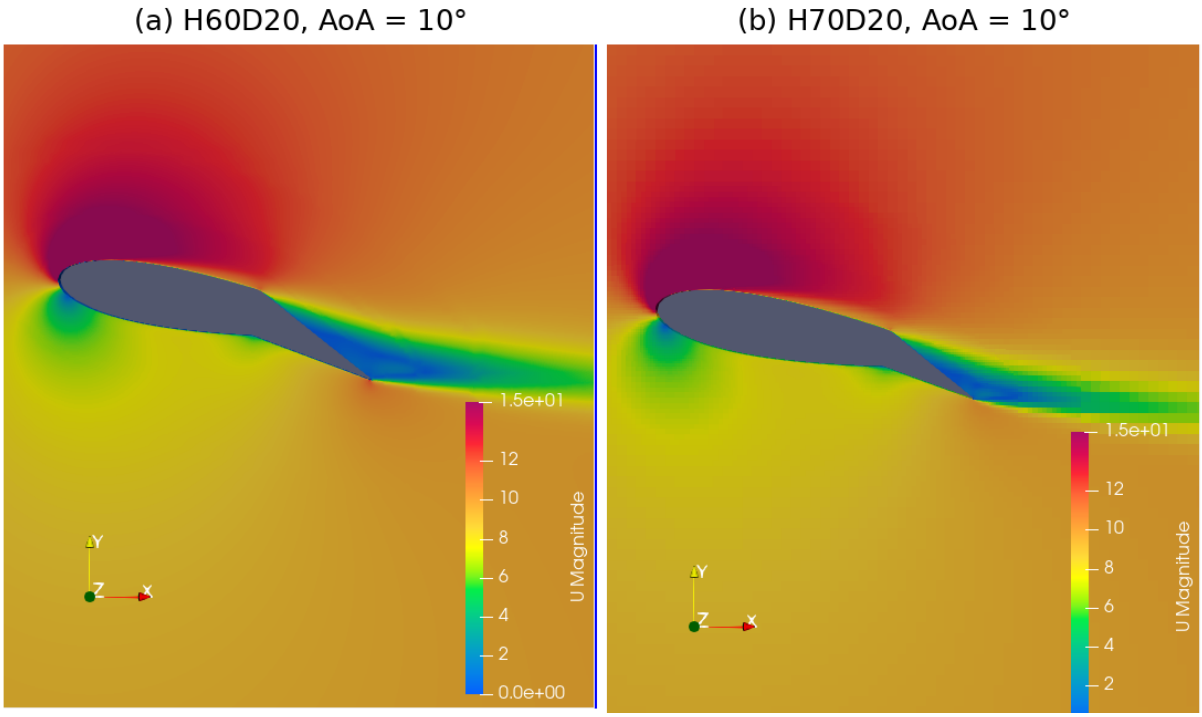

Figure 20: Velocity magnitude contour Comparison between H60D20 and H70D20 at AoA = 10°

around the flap region is greater than in the H70D20 case. This is consistent with the previously discussed coefficient results, in which H60D20 produced higher lift at low AoA. The velocity contour shows the difference in the wake effect near the flap's TE. The wake for the H60D20 is clearer, indicating a stronger disturbance caused by the longer-deflected flap. The H70D20 case produced a less disturbed wake, and these contours support the trends in the lift and drag coefficients.

For the 40° flap deflection cases, H60D40 and H70D40 were stable over the tested AoA range. The H65D40 case had reached stable convergence only up to 15°; hence, the H60D40 and H70D40 cases were used to discuss the effect of the hinge position at larger flap deflection. The results show that the 40° flap deflection produces high lift values for all retained hinge positions and also a clear increase in drag. The large deflection of the flap increases the aerodynamic lift but also has a drag penalty. The effect of hinge position is less consistent than the flap deflection. Therefore, the main conclusion from the 40° case is that the flap deflection has the stronger influence, whereas the hinge position effects should be interpreted more cautiously.

Overall, the hinged flap study shows that increasing flap deflection increases lift but also increases drag. The 40° flap deflection produces the largest aerodynamic lift, while the 20° deflection gives the more moderate increase in lift with a smaller drag penalty. The hinge position also affected the aerodynamic coefficients, but its influence is less direct than that of flap deflection. Therefore, the retained cases suggest that flap deflection is the dominant parameter, while the effects of hinge position require careful interpretation, especially in cases with convergence issues.

4.3 Wingsail Orientation Study

Evaluating the wingsail operating conditions is one of the main objectives of this study. In the previous sections, the aerodynamic performance of the plain airfoil and hinged-flap airfoils was primarily evaluated using the lift and drag coefficients. However, when the wingsail is in the air, the lift and drag are not sufficient to determine whether a particular wingsail configuration is useful, unless the force components, such as thrust and side force, are studied, as explained before in 2.3

The thrust component is important because it can reduce the power required by the main engine. If ship speed can be maintained at a lower engine load, fuel consumption

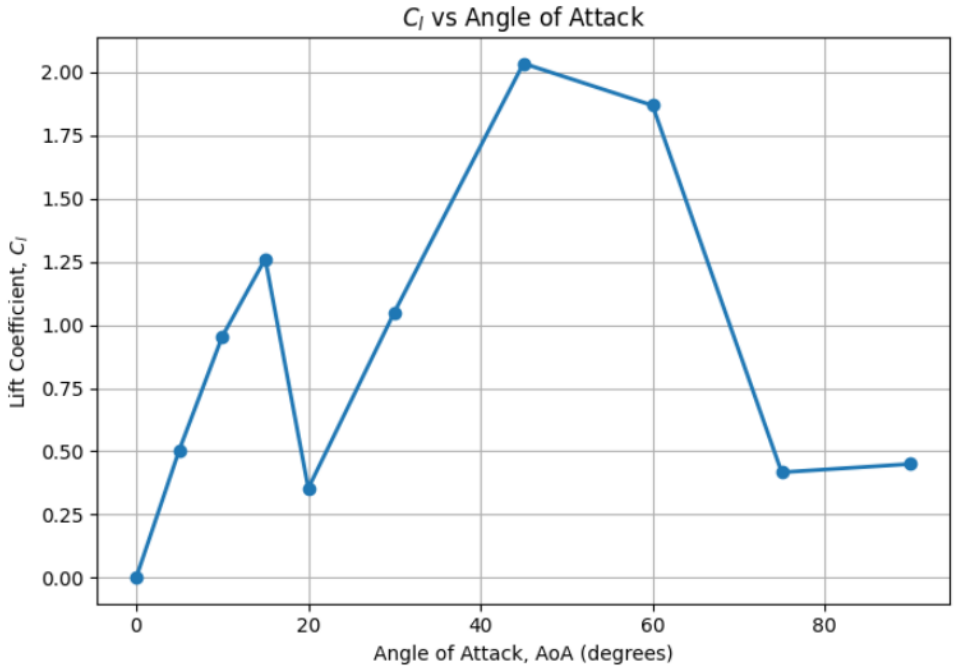

Figure 21: Comparison of C_L vs AoA

and emissions can be reduced. The side force component does not directly impact the propulsion but must be balanced by the hull, rudder, keel, and control system. A large side force increases the yawing moment and hydrodynamic resistance, etc. Therefore, the most useful wingsail condition is not necessarily one with high lift but one that produces high thrust with a reasonable side force.

The first step in this wingsail study was to determine the aerodynamic force coefficients for the plain NACA 0018 airfoil over an AoA range of 0° to 90°. This was necessary because the wingsail can encounter different effective AoA depending upon the apparent wind direction and sail orientation. This allowed the force decomposition to include lift and drag components at the AoA sweep. The simulations were carried out using the same numerical setup described in 4.1.

Figure 21 shows the variation of the lift coefficient with the AoA. The highest lift coefficient increases from low to moderate angles. The results up to 15° AoA were converged and were treated as more reliable for the analysis. Beyond this 15°, the simulations did not converge, and the higher AoAs were not interpreted as fully validated predictions. They are included to provide an approximate trend for the wingsail orientation, where high effective AoA values may occur at large AWAs.

Figure 22 shows the variation of the drag coefficient, where up to the converged range of 15°, the drag coefficient remains relatively low when compared with the higher an-

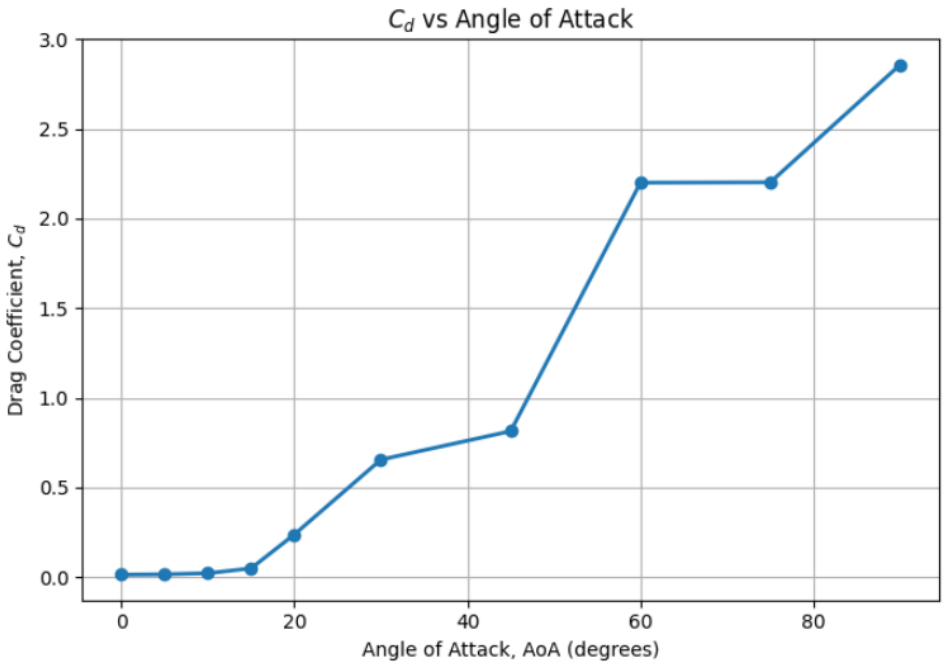

Figure 22: Comparison of C_D VS AoA

gles. The drag increases more drastically than the max lift value as the AoA increases. However, since the results above 15° were not converged, these values were used only as the characteristic data for the post-processing calculation of the C_T, which is the thrust coefficient, and C_S is the side force coefficient.

A simplified mapping approach was used in this wingsail study. CFD simulations were not performed for every AWA and sail orientation angle. Instead, the aerodynamic coefficients from the AoA sweep were used for the force decomposition. Using the angle definitions introduced in Section 2.3, the sail orientation angle was obtained from

$$\theta = \beta - \alpha. \tag{10}$$

For each AWA, all available AoA cases were evaluated. The lift and drag coefficients were then resolved into thrust and side-force coefficients using Equations 8 and 9. The AoA giving the highest thrust coefficient was selected, and the corresponding side-force coefficient was taken from the same operating point. This approach is more suitable than selecting the operating point based only on C_L or C_L/C_D, because the aim of a wingsail is not only to generate lift, but to generate useful thrust in the ship-forward direction.

The selected operating conditions based on the maximum thrust coefficient are shown in Table 4.

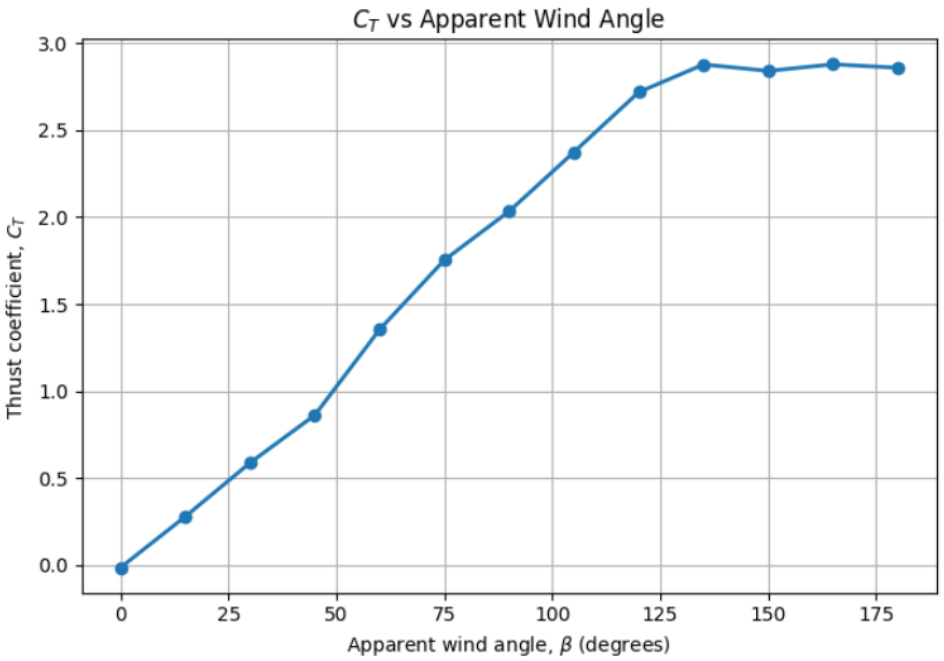

Figure 23: Comparison of Thrust Coefficient C_T vs AWA

Table 4: Selected operating conditions based on maximum thrust coefficient for each AWA.

β (°)	α (°)	θ (°)	C_L	C_D	C_T	C_S	$\lvert C_S \rvert / C_T$
0	0	0	-0.000	0.013	-0.013	-0.000	–
15	15	0	1.261	0.048	0.280	1.231	4.39
30	15	15	1.261	0.048	0.589	1.116	1.89
45	45	0	2.034	0.814	0.863	2.014	2.33
60	45	15	2.034	0.814	1.355	1.722	1.27
75	45	30	2.034	0.814	1.754	1.312	0.75
90	45	45	2.034	0.814	2.034	0.814	0.40
105	60	45	1.868	2.201	2.374	1.642	0.69
120	60	60	1.868	2.201	2.718	0.972	0.36
135	60	75	1.868	2.201	2.877	0.235	0.08
150	60	90	1.868	2.201	2.840	-0.518	0.18
165	90	75	0.450	2.858	2.878	0.305	0.11
180	90	90	0.450	2.858	2.858	-0.450	0.16

The figure 23 should therefore be interpreted as the useful propulsion trends where the thrust is weak at low AWAs and increases through the middle range and reaches the

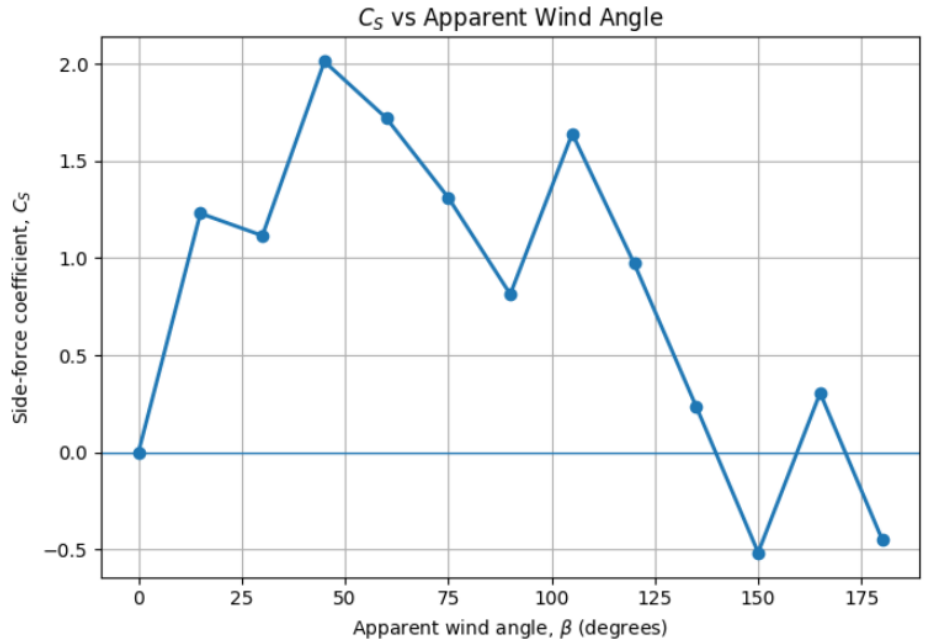

Figure 24: Comparison of side force coefficient C_S vs AWA

highest value at larger AWAs. Figure 24 shows the lateral force, which is relatively large compared with the thrust at low AWAs, but becomes more reasonable in the higher thrust region.

The calculated results show that the thrust coefficient C_T and side force coefficient C_S depend strongly on the AWA, as it determines whether the airfoil section is effective, depending on the wind's direction relative to the ship's direction. At very low AWAs, the apparent wind comes almost from the front of the ship. In this condition, no aerodynamic force produces useful thrust, where at $\beta = 0°$, the maximum C_T is negative. It implies that the aerodynamic force acts against the ship's direction rather than helping it move forward. Hence, this condition is not useful for the wingsail propulsion.

At low AWAs like $\beta = 15°$ and $\beta = 30°$, the wingsail starts to produce the positive thrust. However, it was observed that the side force coefficient remains much larger than the thrust coefficient. It means that most of the aerodynamic forces act sideways instead of forward, which is again not an ideal condition. This side force must be balanced by the hull and rudder, which causes additional resistance. As a result, the wingsail may produce forward force, but it is countered by the side force.

As the AWA increases, the aerodynamic force becomes more useful for propulsion. From around AWA $\beta = 75°$, the thrust coefficient C_T becomes bigger, and the side force becomes reasonable, as a larger part of the aerodynamic force is converted into

useful thrust. This implies that the region where the wingsail becomes more effective can support the ship's forward propulsion without producing excessive side loads.

The highest calculated thrust coefficient occurs at $\beta = 165°$, where $C_T = 2.878$. Using the reference dynamic pressure and reference area from this study, $q_\infty A_{\text{ref}} = 2.5$, this corresponds to an equivalent thrust force of approximately

$$T = C_T q_\infty A_{\text{ref}} = 2.878 \times 2.5 = 7.20 \text{ N}. \tag{11}$$

However, this value occurs at a selected AoA of 90°. At this angle, the airfoil is highly separated and behaves more like a bluff body than an efficient lifting surface. Therefore, although this case gives the highest numerical thrust coefficient, it should not automatically be treated as the best practical operating point.

A more practically favourable region is found between approximately $\beta = 120°$ and $\beta = 150°$. In this range, the thrust coefficient is high while the side-force coefficient is relatively low. For example, at $\beta = 135°$, the selected AoA is 60°, giving $C_T = 2.877$ and $C_S = 0.235$. The equivalent thrust force is:-

$$T = 2.877 \times 2.5 = 7.19 \text{ N}. \tag{12}$$

This is almost the same as the highest calculated thrust at $\beta = 165°$, but the side-force coefficient is lower, and the selected AoA is less extreme. Therefore, $\beta = 135°$ can be considered one of the most favourable operating points in this simplified analysis. It gives very high thrust while keeping the side force comparatively small.

At $\beta = 150°$, the thrust coefficient is also very high with $C_T = 2.840$, which is equivalent to producing a thrust of 7.10 N approximately. The side force coefficient, however, becomes negative, indicating that the lateral force changes direction. The sign convention is not a problem, but it shows that the load direction on the ship changes as the apparent wind approaches the downwind direction. This is important for controlling the wingsail and rudder, as well as structural loading.

From a ship performance perspective, the results suggested that the wingsail has the greatest fuel saving potential in the AWA range where C_T is high, and C_S is relatively low. Considering both thrust and side force, the most favourable operating point in this simplified analysis is around $\beta = 135°$. Under these conditions, the selected AoA is

$\alpha = 60°$, giving $C_T = 2.877$ and $C_S = 0.235$. The equivalent thrust force is approximately 7.19 N, which is almost the same as the highest calculated thrust value, but with a much smaller side-force contribution. Therefore, $\beta = 135°$ provides the best balance between high useful thrust and reasonable side force.

For the shipbuilders and engineers, this type of calculation is useful at the initial stage of the wingsail design. It identifies the wind angle at which the wingsail is most effective and shows that the side force becomes more critical. This is important for estimating the loading on the sail foundation, mast structure, rudder system, etc. The results also suggested that the sail should not just maximize lift force, but it should be controlled to achieve a suitable balance between thrust and side force.Tillig and Ringsberg (2020).

The present results obtained do not directly predict the exact fuel saving of a real ship, as it was not in the scope of this thesis. Therefore, the present analysis should be interpreted as an indication of fuel-saving potential rather than a complete prediction of fuel consumption and cost.

4.4 Gap Sensitivity Analysis

The figure 27 shows the gap size between the main element and the flap element is a very important geometric parameter in multi-element airfoils, as it affects the aerodynamic characteristics between the two elements. The slot allows flow from the pressure side of the main element to the suction side of the flap, thereby modifying the downstream BL and influencing flow separation. The aerodynamic performance of the configurations depends on the balance between increased circulation and viscous losses. Smaller gaps may strengthen the aerodynamic interaction between the elements, while excessively small gaps can increase viscous losses when the wake of the upstream element interacts with the BL of the downstream element van Dam (2002). Previous studies have shown that the gap size can affect drag more strongly than lift at higher AoA Cvetelina Velkova et al. (2015). Based on this background, two gap configurations with $0.018c$ and $0.028c$ were studied and compared with the plain-airfoil baseline.

Figure 25 shows that the plain airfoil produced the highest lift coefficient C_L over the AoA studied. Both slotted-gap configurations generated lower lift than the baseline. For a $0.018c$ gap, the lift coefficient C_L increased from a near-zero value at 0° to its maximum value at 10° and slightly reduced at 15°. The $0.028c$ gap produced lower lift at

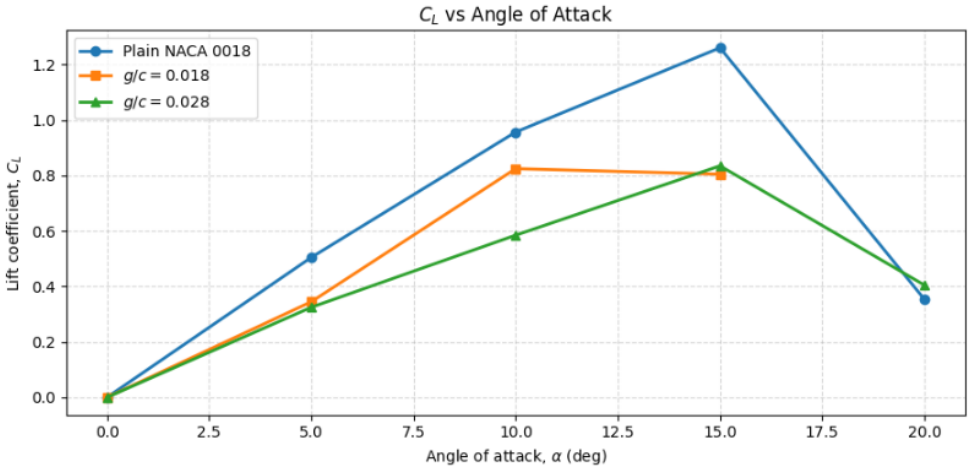

Figure 25: Comparison of C_L for the plain and gap size for NACA 0018 airfoil

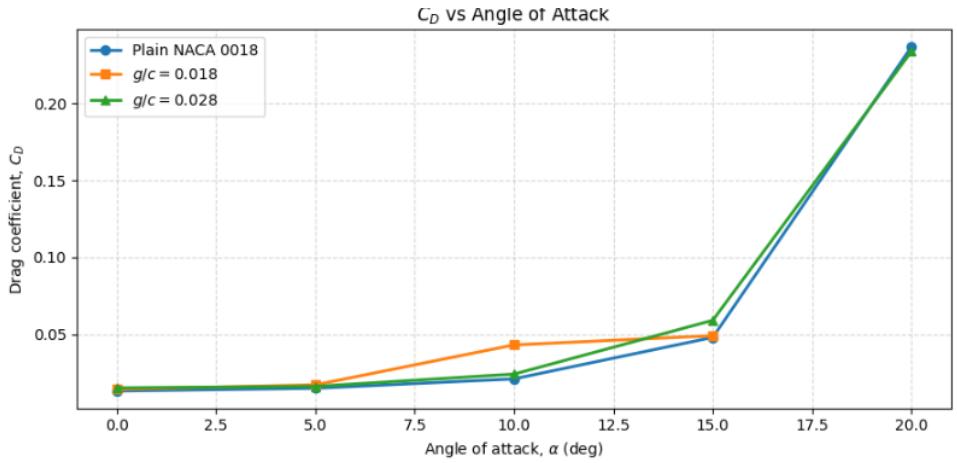

Figure 26: Comparison of C_D for the plain and gap size for NACA 0018 airfoil

the moderate AoA, indicating weaker aerodynamic interaction between the two elements. However, the $0.028c$ gap cases produced a slightly higher lift coefficient C_L at 15° than the $0.018c$ case. Overall, the results show that introducing a slot gap modifies the aerodynamic characteristics but does not improve lift performance relative to the plain-airfoil baseline.

Figure 26 shows that the drag coefficient C_D increases with the AoA. Compared with the plain airfoil, both slotted-gap configurations produced higher drag at moderate and higher AoA. The $0.018c$ gap showed an increase in drag at 10°, but this should be considered carefully, as it does not align with the other AoA trends. The $0.028c$ gap produced lower drag than the $0.018c$ gap at moderate AoA. This suggests that the larger-gap arrangement resulted in a lower drag penalty in this range. However, since no quantitative wake, BL or separation analysis was carried out, the increase in drag should not be directly attributed to viscous interaction or wake effects. Instead, the results show that changing the gap size affects the aerodynamic resistance of the two-element configuration,

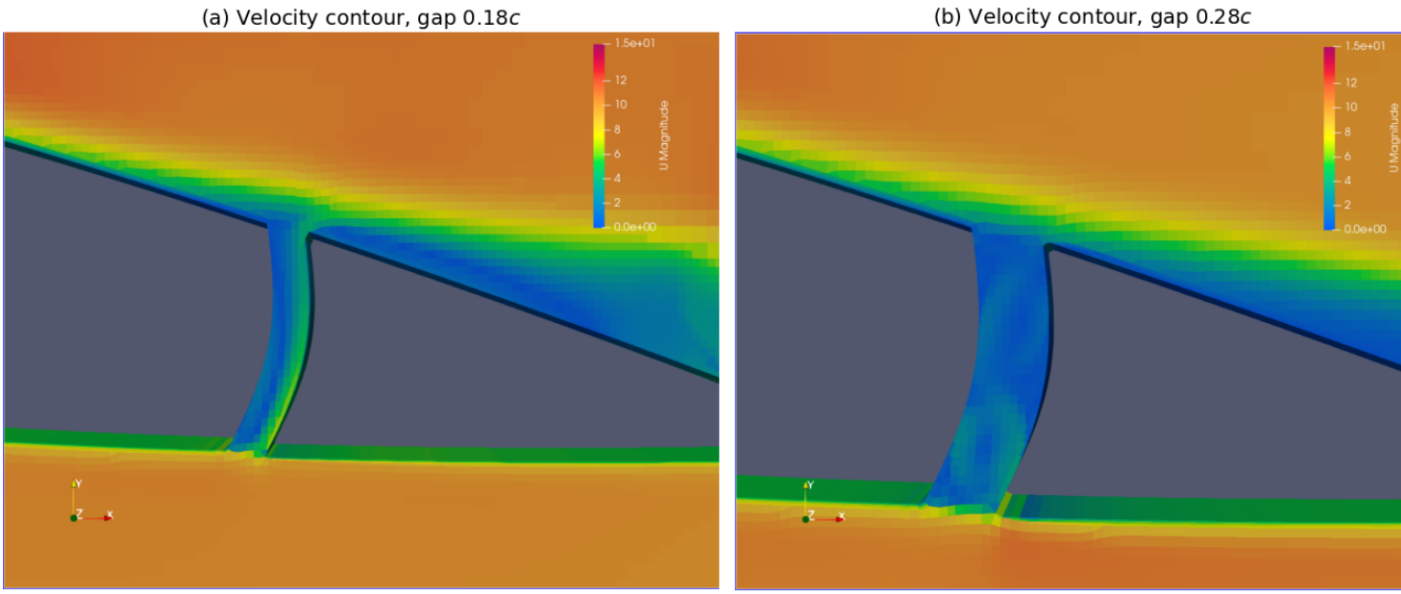

Figure 27: Velocity magnitude contours for gap size 0.018c (left) and 0.028c (right), $\alpha = 10°$

while the influence on lift is comparatively smaller.

Selected velocity contours, shown in Figure 27, were used to qualitatively compare the flow field around the plain airfoil and the gap configurations. At an AoA of 10°, the slotted cases show visible changes in the flow pattern near the gap region and downstream of the flap. For the 0.018c gap, the velocity field indicates local acceleration through the slot region and a more disturbed region behind the two-element configuration compared with the plain airfoil. However, this observation is based only on the contour plot and was not supported by a separate quantitative wake or boundary-layer analysis.

For the 0.028c gap, the downstream flow field appears less concentrated than for the 0.018c gap at the same AoA. This is consistent with the lower drag coefficient observed for the 0.028c case at moderate AoA. However, the contour results should be interpreted qualitatively, since the present study did not calculate wake thickness, momentum deficit, wall shear stress, or separation length. Therefore, the results should not be described as confirmed viscous losses or wake effects. Instead, the contours indicate that changing the gap size modifies the local flow pattern between the main element and the flap, and this is reflected in the aerodynamic coefficient trends.

Overall, the gap sensitivity study showed that the investigated slot gaps significantly changed the aerodynamic behaviour of the airfoil configuration. Both gap configurations increased drag relative to the plain-airfoil baseline. The 0.018c gap produced stronger

drag growth at moderate AoA, whereas the $0.028c$ gap generally led to lower lift generation. Within the investigated range, the plain airfoil baseline retained the best overall aerodynamic efficiency.

5 Analysis and Discussion

The aim of this thesis was to study how AoA, hinged flap geometry, apparent wind direction and gap sizes influence the aerodynamic performance of a NACA 0018-based rigid wingsail section. The results show that the aerodynamic performance of the wingsail cannot be judged from the lift coefficient itself. Although the flap deflections increased the lift coefficient, this improvement came with a drag penalty in several cases, especially at higher AoA. Similarly, the wingsail orientation study showed that high lift force does not necessarily correspond to useful propulsive thrust, because the aerodynamic forces must be resolved into thrust and side-force components relative to the ship's direction.

Therefore, the most important conclusion of this study is not just the configuration with high lift but to optimize the thrust force maintaining the side force at small levels. It is important for WASP that the useful force is the thrust component directed forward. A configuration that produces high aerodynamic forces may still be less suitable if most of it acts sideways or if the drag becomes large.

5.1 Reliability of CFD method and Validation Results

The validation study was used to assess whether the two-dimensional OpenFOAM setup could reproduce the main aerodynamic behaviour of the plain NACA 0018 airfoil before it was applied to the hinged-flap and gap configurations. The validation results showed that the CFD model captured the general increase in lift with AoA and the increase in drag at higher AoA. This behaviour is consistent with basic airfoil theory, in which increasing the AoA strengthens the circulation and increases the pressure difference between the suction and pressure sides until separation becomes significant Anderson (2017).

For the plain NACA 0018 airfoil, the simulation gave approximately zero lift at 0° AoA, which is expected for a symmetric airfoil. From 5° to 15°, the lift coefficient increased with AoA, while the drag coefficient also increased gradually. This indicates that the present setup reproduced the main pre-stall aerodynamic trend of the reference airfoil. Therefore, the validation supports using the numerical method to compare aerodynamic

trends across different wingsail configurations.

However, this should not be interpreted as a complete validation of all flow features. The agreement with reference data is expected to be better at low and moderate AoA than at near-stall AoA. At lower AoA, the flow remains more attached, and the aerodynamic forces are mainly governed by the pressure distribution around the airfoil. In this range, steady RANS simulations with the SST k–ω turbulence model can provide reasonable engineering predictions. At higher AoA, however, the flow becomes more separated and unsteady. Under these conditions, a steady two-dimensional RANS model has more difficulty representing vortex shedding, large-scale separation, and three-dimensional flow effects.

This limitation was observed in the 20° validation case. The case did not achieve acceptable convergence and showed a sharp reduction in lift, accompanied by a large increase in drag. This behaviour is consistent with strong separated flow, but the numerical value itself should not be treated as a reliable quantitative prediction. Therefore, the validation results are considered reliable primarily within the converged range of 0° to 15°. The 20° case is useful for indicating the onset of strong separated behaviour, but it should be interpreted qualitatively.

The mesh independence study also supports the reliability of the numerical setup, but only within practical limits. The results showed that lift and drag coefficients became less sensitive to further refinement after the selected mesh level. The mesh corresponding to `resf = 4` was selected because it provided a good balance between numerical reliability, aerodynamic coefficient convergence, and computational cost. The change in lift and drag between `resf = 4` and the finer mesh was small, indicating that further refinement did not significantly change the aerodynamic coefficients.

However, mesh independence does not mean that the simulation is exact. It only shows that the numerical solution was not strongly changed by further mesh refinement within the tested range. The y^+ values and near-wall treatment remain important, especially because wall-bounded separation and adverse pressure gradients strongly affect drag and stall behaviour. The average y^+ value was similar across the tested meshes, but the minimum and maximum values should also be considered, as the local near-wall resolution can influence separation prediction. Therefore, the final CFD method should be considered suitable for comparative aerodynamic analysis, but not for exact full-scale

prediction of wingsail or ship performance.

Another important limitation is that the simulations were two-dimensional. Real wingsails have a finite span, tip effects, structural supports, and interaction with the ship deck and superstructure. These effects cannot be captured in the current model. The results are therefore best interpreted as sectional aerodynamic trends rather than direct predictions of a complete ship-mounted wingsail. This limitation is acceptable for comparing hinge position, flap deflection, and gap effects, but it should be considered before using the results in the final design.

5.2 Influence of Hinged-Flap Deflection and Hinge Position

The hinged-flap study showed that flap deflection strongly influences the aerodynamic coefficients. Increasing flap deflection increased the airfoil's effective camber, thereby increasing the lift coefficient over most of the investigated angle-of-attack range. This is consistent with high-lift theory and previous studies on flapped airfoils, in which trailing-edge deflection increases circulation and shifts the lift curve.

However, the increase in lift was also accompanied by an increase in drag. This drag penalty is caused by stronger adverse pressure gradients, increased curvature of the flow around the flap, and stronger wake development behind the trailing edge. As the flap deflection increases, the airfoil produces more lift, but the rear part of the geometry also becomes a stronger source of pressure drag and separated flow. This means that flap deflection is beneficial only up to the point where the lift increase is not outweighed by the drag penalty.

The 20° flap deflection produced a moderate increase in lift while keeping the drag increase smaller than in the 40° flap cases. This suggests that moderate flap deflection may provide a better compromise for practical operation. In contrast, the 40° flap deflection generated larger lift, but it also caused a stronger drag penalty and more separated flow. Therefore, the 40° flap case is useful when maximum lift is desired, but it is not necessarily the most efficient condition for propulsion. For a wingsail, where the useful output is forward thrust rather than lift alone, the additional drag must be considered.

The effect of hinge position was less direct than the effect of flap deflection. Moving the hinge position changes the effective flap length. A hinge located further forward, such as H60, creates a longer movable flap than H70. This can increase the flap's aerodynamic

influence because a larger portion of the airfoil is deflected. Therefore, the H60 cases generally produced greater changes in pressure distribution and wake behaviour than the H70 cases at the same flap deflection.

The comparison between H60D20 and H70D20 at the same AoA showed that the longer flap produced stronger pressure and velocity changes near the rear part of the airfoil. The H60D20 case showed a stronger pressure difference around the flap region and a more visible wake behind the trailing edge. This supports the idea that hinge position affects the local flow structure and wake development by changing the effective length of the deflected flap.

However, the hinge-position trend was not as consistent as the flap-deflection trend. Some hinge configurations showed convergence issues or were excluded because the generated geometries were not suitable for the CFD study. For example, the H65D20 case did not reach acceptable convergence and was excluded from the quantitative comparison. This means that the hinge-position results should be interpreted with caution. The geometry near the hinge and the quality of the mesh around the deflected flap can strongly affect the numerical solution.

For this reason, the present results support the conclusion that flap deflection is the dominant parameter, while hinge position requires further investigation with improved geometry control, mesh refinement near the hinge, and additional simulations. The results show the general trend that moving the hinge forward can strengthen the flap effect, but they do not provide enough evidence to define one optimum hinge position for all operating conditions.

5.3 Interpretation of Thrust and Side Force

The wingsail-orientation study is important because it connects the airfoil force coefficients to ship propulsion. In ordinary airfoil analysis, lift and drag are defined relative to the incoming flow. However, for a ship, the useful force is the component acting in the forward direction of travel. This means that high lift does not automatically mean high thrust. Depending on the apparent wind direction, a large part of the aerodynamic force may act sideways instead of forward.

The results showed that the thrust coefficient depends strongly on the AWA and the selected AoA. At low AWAs, the wingsail produced weak or even negative thrust because

the aerodynamic force was not favourably aligned with the ship's direction. Under these conditions, the aerodynamic loading may exist, but it does not contribute effectively to forward propulsion. This shows why lift coefficient alone is not sufficient for evaluating wingsail performance.

As the AWA increased, a larger part of the aerodynamic force contributed to forward thrust. This led to higher thrust coefficients at moderate and large AWAs. However, the side-force coefficient also changed with AWA. At some apparent wind directions, the airfoil generated a large resultant aerodynamic force, but a significant part of this force acted laterally. This is not always desirable because side force can increase leeway, yawing moment, heeling load, and additional hydrodynamic resistance. Therefore, the most favourable operating condition is not simply the one with the highest thrust coefficient, but the one that gives a high thrust coefficient while keeping the side force at a manageable level.

In the simplified analysis, the operating region around 135° AWA gave a favourable balance between thrust and side force. This condition produced a high thrust component while avoiding the largest side-force penalty. This result supports the main argument of the thesis: a wingsail should not be controlled only to maximise lift. Instead, the control strategy should aim to maximise useful thrust while limiting drag and side loading. This agrees with the practical requirements of wind-assisted ship propulsion, where the aerodynamic benefit must be balanced against structural loads, manoeuvrability, and ship stability

However, the orientation study should be interpreted as a simplified post-processing analysis. The force decomposition was based on two-dimensional airfoil coefficients and did not include the full ship hull, rudder response, sail height, heeling moment, or control limitations. In a real ship application, the optimum sail angle would also depend on ship speed, true wind speed, true wind angle, sea state, route, and the interaction between the sail and the vessel.

Another important point is that some of the highest calculated thrust values were obtained at high effective AoA. These high-angle-of-attack cases are less reliable because the CFD simulations did not show the same convergence quality as the lower-angle cases. Under these conditions, the airfoil is expected to be strongly separated and may behave more like a bluff body than an efficient lifting surface. Therefore, although the mathematical

force decomposition may give high thrust values, these points should not automatically be treated as practical operating points.

The most useful interpretation is that the wingsail has the greatest potential when the AWA allows a large part of the aerodynamic force to act in the ship-forward direction while keeping the side force reasonably low. Therefore, the orientation study should be seen as an indication of useful operating regions rather than a complete sail-control optimisation.

5.4 Effect of Gap Size in the Multi-Element Configuration

The gap sensitivity study showed that the investigated slot gaps changed the aerodynamic behaviour of the airfoil. In theory, a slot between a main element and a flap can improve lift by allowing higher-energy flow to pass through the gap and re-energize the boundary layer on the downstream element. This can delay separation and improve the pressure distribution on the flap. However, the aerodynamic benefit of a slot depends strongly on the size and position of the gap, the overlap between the elements, and the flap angle

In the present study, the gap configurations did not automatically improve the overall aerodynamic performance. However, this conclusion is mainly limited to the small number of cases considered in this study. Only two gap sizes were evaluated, and the results should therefore not be interpreted as a general conclusion for all possible slotted-airfoil designs. For the cases studied here, both gap configurations increased drag relative to the plain-airfoil baseline. The smaller gap produced greater drag growth at moderate AoA, suggesting stronger viscous interaction and wake development between the main element and the flap. The velocity contours also showed stronger flow acceleration through the slot and a more disturbed downstream wake. This indicates that the gap not only modified the pressure distribution but also increased losses in the wake region.

The larger gap showed a different behaviour. It produced weaker interaction between the two elements and generally lower lift generation at moderate AoA. This suggests that the gap became too large to maintain a strong beneficial slot effect. Instead of improving the flap performance, the larger gap reduced the aerodynamic coupling between the main element and the flap. As a result, the plain baseline remained more efficient within the investigated range.

This result is important because it shows that multi-element airfoils are sensitive to geometric details. Adding a slot or gap does not guarantee better aerodynamic perfor-

mance. Larger gaps may have a stronger influence on the aerodynamic interaction between the main element and the flap because they change the spacing between the elements. Similar observations have been made in previous studies of multi-element airfoils, where gap size was shown to influence both lift and drag behaviour.

For the present thesis, the gap study should therefore be presented as an initial sensitivity analysis rather than a final optimisation. The investigated gaps altered the flow field but did not improve aerodynamic efficiency relative to the plain-airfoil baseline. A more complete gap optimisation would require a larger design matrix including gap distance, overlap, flap deflection, and AoA. The local mesh quality in the gap region would also need to be carefully checked, as small geometric changes there can strongly affect the flow solution.

5.5 Limitations of the Present Study

Several limitations affected the interpretation of the results. First, the simulations were limited to two-dimensional steady RANS. This approach is useful for comparing many configurations at reasonable computational cost, but it cannot capture all unsteady and three-dimensional flow structures. This is especially important near the stall, where vortex shedding, separated flow, and spanwise flow may dominate the aerodynamic forces.

Second, some configurations had convergence difficulties. This was particularly relevant for large flap deflections, high AoA, and certain hinge positions. If the residuals and force histories do not stabilise, the calculated coefficients should not be treated as fully reliable. These cases are still useful for identifying problematic geometries and flow regimes, but they should not be used as the main basis for design conclusions.

Third, the study used a limited range of hinge positions, flap angles, and gap sizes. The selected cases show important trends, but they do not represent a complete optimisation of the wingsail geometry. Other combinations of hinge position, flap length, flap deflection, gap size, and overlap may produce better performance. Therefore, the results should be interpreted as a comparative investigation of selected configurations rather than a final optimised design.

Fourth, the geometry generation process affected which cases could be studied. Some hinge positions were removed because the generated geometries were unsuitable for meshing or produced poor-quality regions near the hinges. This is an important practical

limitation because the aerodynamic performance of a hinged flap depends not only on the selected hinge location but also on whether the resulting geometry is smooth, meshable, and physically reasonable.

Fifth, the study did not include a full ship model. The thrust and side-force analysis was based on aerodynamic force decomposition rather than a coupled aero-hydrodynamic simulation. In practice, the net benefit of a wingsail depends on how the aerodynamic forces interact with the ship hull, rudder, stability, route, and control system. Therefore, the present results should be interpreted as aerodynamic indicators rather than direct fuel-saving predictions.

Finally, the results are based on a fixed inflow condition and a simplified two-dimensional reference area. Real operating conditions would involve changing wind speed, AWA, ship motion, atmospheric turbulence, and control-system response. These effects were outside the scope of this thesis, but they would be important for practical wingsail design.

5.6 Implications for Wingsail Design

The results have several implications for rigid wingsail design. First, flap deflection is an effective means of modifying the aerodynamic performance of a rigid wingsail section. Moderate flap deflection can improve lift without causing as large a drag penalty as high flap deflection. This suggests that a smaller flap deflection may be more useful in practice if it provides sufficient thrust while keeping drag and wake development lower.

Second, hinge position affects the pressure distribution and wake structure, but its influence is more sensitive to geometry and convergence quality. A hinge located farther forward increases the effective flap length and can strengthen the flap's aerodynamic effect. However, this can also increase drag and separation. Therefore, hinge position should not be selected independently. It should be designed together with the flap deflection angle, the expected operating AoA, and the structural constraints.

Third, the best aerodynamic configuration for ship propulsion is not necessarily the one with the highest lift coefficient. The thrust and side-force balance must be considered. A wingsail operating condition with slightly lower lift may be more favourable if it produces lower drag and smaller side force. This is especially important for ship applications, where excessive side force can increase rudder demand, yawing moment, heeling load, and structural requirements.

Fourth, the gap sensitivity results show that multi-element configurations require careful design. A poorly selected gap can increase drag and reduce aerodynamic efficiency. Therefore, the gap size should not be chosen only from geometric convenience. It should be optimised together with flap angle, hinge position, overlap, and apparent wind direction.

Overall, the present study provides a useful CFD-based comparison of different wingsail configurations. The results show that hinged flaps can improve aerodynamic performance, but the benefit depends strongly on the balance between lift increase, drag penalty, thrust direction, side-force loading, and flow separation. This supports the need for wingsail design methods that evaluate the complete aerodynamic force system rather than lift alone.

5.7 Recommendations for Future Work

Future work should first extend the present two-dimensional study with a more systematic parametric investigation. More hinge positions, smaller increments in flap deflection, and additional gap sizes should be tested. This would allow clearer identification of the range in which flap deflection improves thrust without producing excessive drag or side force.

A second step should be to improve the treatment of separated flow. Since the present steady RANS setup showed convergence limitations at high AoA, unsteady RANS or LES could be used for selected cases where wake dynamics and stall behaviour are important. This would be especially relevant for the wingsail-orientation study, where some high-thrust operating points were based on high effective AoA.

A third step should be to perform three-dimensional simulations. A finite-span wingsail would include tip effects, spanwise flow, and more realistic loading distributions. This would make the aerodynamic coefficients more representative of practical wingsail operation. In addition,the aerodynamic forces should eventually be coupled with a simplified ship model to estimate how thrust, side force, yaw moment, heel, and hydrodynamic resistance interact.

Further work should also include a more detailed gap optimisation study. The present study only considered selected gap configurations, but multi-element airfoil performance depends strongly on gap size, overlap, flap angle, and element alignment. A wider design matrix would help identify whether a better gap arrangement can improve lift without causing excessive drag.

Finally, experimental validation would improve confidence in the numerical results. Wind-tunnel testing of selected flap and gap configurations could provide force measurements and flow visualisation for comparison with the CFD results. This would be particularly useful for cases involving separation, where numerical predictions are more uncertain.

Overall, the present study shows that hinged flaps can improve the aerodynamic force generation of a rigid wingsail section, but the improvement must be assessed using more than just the lift coefficient. The most useful wingsail configuration is not necessarily the one with the highest lift, but the one that provides useful thrust with acceptable drag, side force, and flow stability. This conclusion supports the need for wingsail optimisation methods that combine airfoil aerodynamics, force decomposition, and practical ship-operation constraints.

6 Conclusions

This thesis investigated the aerodynamic performance of a NACA 0018-based rigid wingsail section using two-dimensional CFD simulations in OpenFOAM. The study focused on the effects of AoA, hinged flap deflections and hinge position, AWA, and gap size on the lift coefficient C_L, drag coefficient C_D, thrust coefficient C_T, side-force coefficient C_S, and the surrounding flow behaviour. The main purpose was not just to identify the configurations with high lift coefficient C_L, but also to understand whether the generated aerodynamic force can contribute usefully to the WASP.

The validation study showed that the numerical setup was able to reproduce the main aerodynamic trends of the plain NACA 0018 airfoil in the converged AoA range from 0° to 15°. In this range, the lift coefficient C_L increased with AoA, while the drag coefficient C_D also increased gradually. This behaviour agreed with the expected response of a symmetric airfoil before strong stall effects occur. The 20° case did not reach acceptable convergence and was therefore interpreted only qualitatively. This showed that the steady two-dimensional RANS setup is suitable for comparing pre-stall and moderately separated aerodynamic trends, but less reliable for strongly separated high-AoA cases.

The hinged-flap study showed that flap deflection has a strong influence on aerodynamic performance. Increasing the flap deflection increased the effective camber of the airfoil and produced a higher lift coefficient C_L. However, this improvement was accom-

panied by an increased drag coefficient C_D and stronger wake development. The 20° flap deflection gave a moderate lift increase with a smaller drag penalty, while the 40° flap deflection produced higher lift but also much larger drag. Therefore, the configuration with the highest lift coefficient C_L was not exactly the most efficient or useful configuration when it comes to propulsion.

The hinge-position study showed that moving the hinge position does changes the effective flap length and therefore affects the pressure distribution and wake behaviour. A smaller hinge position, like the H60, creates a longer deflected flap and produces stronger aerodynamic characteristics than H70 at the same flap deflection of 20°. However, the hinge-position effect was not so consistent when compared to the flap-deflection because some configurations having geometry and convergence issues. Therefore, flap deflection was found to be the important parameter in the present thesis, while hinge position requires further investigation before an optimum location can be defined.

The wingsail-orientation study showed that the lift coefficient C_L alone is not sufficient for evaluating wingsail performance. For the propulsion of the ship, the aerodynamic force was resolved into thrust and side-force components relative to the ship's direction. The results showed that low AWAs produced a weak or even negative thrust coefficient C_T, whereas larger AWAs enabled a greater portion of the aerodynamic force to contribute to forward propulsion. In the simplified analysis, the operating region around $\beta = 135°$ gave a favourable balance between high thrust coefficient C_T and manageable side-force coefficient C_S. However, some high-thrust-coefficient points were based on high effective AoA values and should be interpreted qualitatively because these cases involved stronger separation and lower convergence reliability.

The gap sensitivity study showed that the investigated gap configurations changed the flow behaviour but did not improve the overall aerodynamic efficiency compared with the plain-airfoil baseline. The gap cases generally increased the drag coefficient C_D and did not produce a higher lift coefficient C_L than the plain airfoil in the tested range. The $0.018c$ gap produced stronger drag growth at moderate AoA, while the $0.028c$ gap produced lower lift generation. This implied that adding a slot or gap does not automatically improve performance. The aerodynamic effects thus depends strongly on gap size, overlap, flap angle, and element interaction. Therefore, the gap study should be understood as an initial sensitivity analysis rather than a complete multi-element optimisation.

Overall, the thesis shows that hinged TE flaps can improve the aerodynamic force generation of a rigid wingsail section, but their usefulness depends on the balance between lift increase, drag penalty, thrust coefficient C_T, side-force coefficient C_S, and flow separation. The most suitable wingsail configuration is not necessarily the one with the highest lift coefficient C_L. Instead, a useful design should provide sufficient thrust coefficient C_T while maintaining acceptable drag, side force, and flow stability. The results should be interpreted as section-wise aerodynamic trends rather than full-scale ship performance predictions. Future work should include a wider parametric study, unsteady and three-dimensional simulations, and additional experimental validation for those configurations.

References

Ahmed, T., Amin, M. T., Islam, S. M. R., and Ahmed, S. (2013). Computational study of flow around a NACA 0012 wing flapped at different flap angles with varying mach numbers. *Global Journal of Researches in Engineering: General Engineering*, 13(4):5–14. Version 1.0.

AirfoilTools (2026). NACA 0018 (naca0018-il) XFOIL prediction polar at Re = 200,000 and Ncrit = 9. Accessed: 16 February 2026.

Ali, B., Ouahiba, G., Hamid, O., and Ahmed, B. (2018). Aerodynamic optimization of active flow control over S809 airfoil using synthetic jet. In *2018 International Conference on Wind Energy and Applications in Algeria (ICWEAA)*, pages 1–6, Algiers. IEEE.

Anderson, J. D. (2017). *Fundamentals of Aerodynamics*. McGraw-Hill Education, New York, NY, 6 edition.

Arra, A., Anekar, N., and Nimbalkar, S. (2021). Aerodynamic effects of leading edge (le) slats and slotted trailing edge (te) flaps on naca-2412 airfoil in prospect of optimization. *Materials Today: Proceedings*, 44(Part 1):587–595.

Chen, J., Ye, Z., Yang, R., Cai, G., Li, J., and Li, H. (2018). Design and Control of Multiple Wing-sail Land Yacht Robot. In *2018 IEEE International Conference on Mechatronics and Automation (ICMA)*, pages 1800–1805, Changchun. IEEE.

Cvetelina Velkova, Michael Todorov, and Guillaume Durand (2015). Study the Influence of a Gap between the Wing and Slotted Flap over the Aerodynamic Characteristics of Ultra-Light Aircraft Wing Airfoil. *Journal of Mechanics Engineering and Automation*, 5(5).

De Marco, A., Mancini, S., Pensa, C., Calise, G., and De Luca, F. (2016). Flettner Rotor Concept for Marine Applications: A Systematic Study. *International Journal of Rotating Machinery*, 2016:1–12.

Ding, T., Tian, C., Wang, H., Xu, C., Ye, J., Gong, A., Liu, M., and Xia, T. (2025). Performance enhancement of autonomous sailboats via cfd-optimized wing–tail sail configurations. *Journal of Marine Science and Engineering*, 13:1640.

Eggert, C. A. and Rumsey, C. L. (2017). CFD Study of NACA 0018 Airfoil with Flow Control. NASA Technical Memorandum NASA/TM–2017–219602, National Aeronautics and Space Administration, Hampton, Virginia.

Fang, S., Tian, C., Zhang, Y., Xu, C., Ding, T., Wang, H., and Xia, T. (2024). Aerodynamic Analysis of Rigid Wing Sail Based on CFD Simulation for the Design of High-Performance Unmanned Sailboats. *Mathematics*, 12(16):2481.

Fatahian, E., Lohrasbi Nichkoohi, A., Salarian, H., and Khaleghinia, J. (2020). Effects of the hinge position and suction on flow separation and aerodynamic performance of the NACA 0012 airfoil. *Journal of the Brazilian Society of Mechanical Sciences and Engineering*, 42(2):86.

Gaul, K. and Rutkowski, G. (2025). Harnessing the Wind: The Rise of Wind-Assisted Ship Propulsion (WASP) in the Transformation of Maritime Transport. *TransNav, the International Journal on Marine Navigation and Safety of Sea Transportation*, 19(1):217–225.

Hoffmeister, H., Hollenbach, U., Tranell, J., Aalbu, K., Skåre, O. G., and Endresen, Ø. (2025). Wind-assisted propulsion systems (WAPS): How WAPS can help to comply with GHG regulations. White paper, DNV. Project team/reviewers include Jason Stefanatos, Jan Kvålsvold, Håkon Hustad, Tore Longva, Jan Wienke, Marius Leisner and Jeannette Schäfer.

Jiang, Y., Cao, C., Cui, T., Yang, H., and Tian, Z. (2024). Numerical Study on Auxiliary Propulsion Performance of Foldable Three-Element Wingsail Utilizing Wind Energy. *Energies*, 17(15):3833.

Kamliya Jawahar, H., Ai, Q., and Azarpeyvand, M. (2018). Experimental and numerical investigation of aerodynamic performance for airfoils with morphed trailing edges. *Renewable Energy*, 127:355–367.

Khan, L., Macklin, J. J. R., Peck, B. C. D., Morton, O., and Souppez, J.-B. R. G. (2021). A REVIEW OF WIND-ASSISTED SHIP PROPULSION FOR SUSTAINABLECOMMERCIAL SHIPPING: LATEST DEVELOPMENTS AND FUTURE STAKES. *Wind Propulsion 2021*.

Kolodziejski, M. and Sosnowski, M. (2025). Review of Wind-Assisted Propulsion Systems in Maritime Transport. *Energies*, 18(4):897.

Kuang, L., Li, H., Su, X., Song, X., Wang, Z., Zhang, Y., and Ma, W. (2023). Effect of chord length ratio on aerodynamic performance of two-element wing sail. *Ocean Engineering*, 287:115946.

Lee, H., Jo, Y., Lee, D.-J., and Choi, S. (2016). Surrogate model based design optimization of multiple wing sails considering flow interaction effect. *Ocean Engineering*, 121:422–436.

Li, C. and Yang, J. (2016). Flight control using only synthetic jet actuators in high-angle-of-attack. In *2016 35th Chinese Control Conference (CCC)*, pages 10662–10667, Chengdu. IEEE.

Ma, R., Li, D., Zhang, R., Tian, F., Tang, Z., Cao, J., Xie, Y., Jing, Z., Chen, J., Li, X., and Huang, L. (2025). Arrangement optimization of wingsails subject to complex mutual aerodynamic interference: A numerical study. *Ocean Engineering*, 342:122919.

Makram, T. E., Panagiotou, P., and Mattheou, D. (2023). Wingsail layout design and shape optimization using a CFD-aided Taguchi approach: The Aegean Marathon case study. *Ocean Engineering*, 276:114055.

Malmek, K., Larsson, L., Werner, S., Ringsberg, J. W., Bensow, R., and Finnsgård, C. (2024). Rapid aerodynamic method for predicting the performance of interacting wing sails. *Ocean Engineering*, 293:116596.

Morris, W. J. and Rusak, Z. (2013). Stall onset on aerofoils at low to moderately high Reynolds number flows. *Journal of Fluid Mechanics*, 733:439–472.

Obeid, S., Jha, R., and Ahmadi, G. (2017). Rans simulations of aerodynamic performance of naca 0015 flapped airfoil. *Fluids*, 2:2.

OpenCFD Ltd. (2023a). *OpenFOAM v2306 User Guide: noSlip boundary condition*. OpenCFD Ltd. Accessed: 3 June 2026.

OpenCFD Ltd. (2023b). *OpenFOAM v2306 User Guide: nutkWallFunction boundary condition*. OpenCFD Ltd. Accessed: 3 June 2026.

OpenCFD Ltd. (2023c). *OpenFOAM v2306 User Guide: RAS wall functions*. OpenCFD Ltd. Accessed: 3 June 2026.

Schlichting, H. and Gersten, K. (2017). *Boundary-Layer Theory*. Springer Berlin Heidelberg, Berlin, Heidelberg.

Seifert, J. (2012). A review of the Magnus effect in aeronautics. *Progress in Aerospace Sciences*, 55:17–45.

Tillig, F. and Ringsberg, J. W. (2020). Design, operation and analysis of wind-assisted cargo ships. *Ocean Engineering*, 211:107603.

van Dam, C. P. (2002). The aerodynamic design of multi-element high-lift systems for transport airplanes. *Progress in Aerospace Sciences*, 38(2):101–144.

Von Klemperer, C. J., Horwitz, R. A., and Malan, A. G. (2023). An articulating wingsail design for Wind Assisted Ship Propulsion (WASP) applications. *Scientific African*, 20:e01699.

Vos, R. and Farokhi, S. (2015). *Introduction to Transonic Aerodynamics*, volume 110 of *Fluid Mechanics and Its Applications*. Springer Netherlands, Dordrecht.

Wang, H., Li, C., Zuo, C., Yuan, J., and Wu, B. (2024). Computational Fluid Dynamics Investigation of the Spacing of the Aerodynamic Characteristics for Multiple Wingsails on Ships. *Journal of Marine Science and Engineering*, 12(6):985.

Xu, K., Malmek, K., and Bensow, R. (2025). Numerical investigation of multiple wingsails interaction under different apparent wind angles. *Ocean Engineering*, 336:121712.

Zhang, R., Huang, L., Peng, G., Ruan, Z., Ma, R., Wang, K., Cao, J., Wu, J., and Li, X. (2025). Investigation of aerodynamic performance and operational optimization of wing sails at varying spacings. *Ocean Engineering*, 333:121444.